



SMASH v1.0: A Differentiable and Regionalizable High-Resolution Hydrological Modeling and Data Assimilation Framework

François Colleoni¹, Ngo Nghi Truyen Huynh¹, Pierre-André Garambois¹, Maxime Jay-Allemand², Didier Organde², Benjamin Renard¹, Thomas De Fournas¹, Apolline El Baz¹, Julie Demargne², and Pierre Javelle¹

¹INRAE, Aix-Marseille Université, RECOVER, 3275 Route Cézanne, 13182 Aix-en-Provence, France

²HYDRIS Hydrologie, Parc Scientifique Agropolis II, 2196 Boulevard de la Lironde, 34980 Montferrier-sur-Lez, France

Correspondence: Pierre-André Garambois (pierre-andre.garambois@inrae.fr)

Abstract. The `smash` software is a differentiable and regionalizable framework enabling modular high-resolution hydrological modeling and data assimilation, from catchment to regional and country scales, for water research and operational applications. `smash` combines various process-based conceptual operators for vertical and lateral flows, which can be hybridized with a descriptors-to-parameters neural network for regionalization. `smash` features an efficient, differentiable Fortran solver using Tapenade that supports CPU parallel computing and spatially distributed optimization of large parameter vectors, interfaced in Python using `f90wrap`. This article presents `smash` algorithms, their open-source code, documentation and tutorials. It highlights foundational research, benchmarking on state-of-the-art datasets, and readiness for scientific and operational use. To ensure reproducibility, open-source datasets are used to demonstrate the main functionalities of `smash`, including parallel computation performances and the application of multiple spatially distributed conceptual model structures over a large catchment sample. These functionalities include uniform or spatially distributed calibration and regionalization by learning the relation between descriptors and parameters. Provided Python tool allows application to any other catchment from globally available datasets. Using CAMELS, as per recent articles, median $KGE > 0.8$ are obtained in local spatially distributed calibration for daily GR-like and VIC-like model structures at $dx = 1'30''$ ($\sim 3km$), and $KGE > 0.6$ in spatio-temporal validation in a regionalization context. The regionalization of a high resolution hourly GR-like model structure at $dx = 500m$ over a difficult mediterranean flash-flood prone case results in $NSE > 0.6$ in spatio-temporal validation. The proposed differentiable and regionalizable spatially distributed modeling framework is designed for variational data assimilation and is intended for collaborative research and operational applications. Additionally, `smash` supports the implementation of other differentiable hydrological and hydraulic models, as well as hybrid physics-AI models, further enhancing its versatility and applicability.

1 Introduction

Hydrological models are indispensable tools for hydrosystems functioning understanding, floods and low flows forecasting, sustainable water management and infrastructure design, environmental protection, and adaptation to a changing climate. Indeed, measurements of hydrological responses are not ubiquitously available (e.g. Beven (2011)) while "everywhere relevant"



(Bierkens et al., 2015) estimation of hydrological state-fluxes is expected. A model is hence needed to extend and predict those quantities of interest based on available data.

25 High-resolution spatial datasets have become increasingly accessible, often on a global scale, and enable describing topography-soil-vegetation properties as well as atmospheric variables. Examples include the ECMWF atmospheric reanalysis version 5 (ERA5) (Hersbach et al., 2020) and rainfall product MSWEP (Beck et al., 2019), flow directions IHU (Eilander et al., 2021) from MERIT terrain elevations (Yamazaki et al., 2017), the SoilGrids pedology (Hengl et al., 2017), daily discharge from Caravan-CAMELS (Kratzert et al., 2023; Addor et al., 2017), that will be used hereafter. Such data can be directly exploited by
 30 grid based spatially distributed hydrological models, whose development at "hyper-resolution" (1km^2 or finer) is recognized as a "grand challenge for hydrology" to address water problems facing society (Wood et al., 2011; Bierkens et al., 2015).

Hydrological responses result from combined non-linear vertical and lateral physical processes occurring at multiple scales in the critical zone and their limited observability (e.g. Beven, 1989; Milly, 1994; Blöschl and Sivapalan, 1995; Refsgaard, 1997; Vereecken et al., 2019) makes hydrological modeling uncertain and difficult (e.g. Liu and Gupta, 2007)). In the absence
 35 of directly exploitable first principles in hydrology (e.g., Dooge (1986)), as opposed to flow mechanistic equations in continuous media such as river hydraulics, meteorology or oceanography, and given the high heterogeneities of continental hydrosystems compartments and the lack of "scale-relevant theories" (Beven, 1987), process-based hydrological models generally include a certain amount of empiricism. It represents an avenue for the fusion of data assimilation (DA) and uncertainty quantification (UQ) with machine learning (ML) and deep learning (DL) techniques to better exploit the informative richness of multi-source
 40 data.

Differentiability of the forward numerical model is a key technology to achieve, for gradient based optimization of large parameter vectors (e.g. variational data assimilation in 2D or 1D hydraulic models (Monnier et al., 2016; Brisset et al., 2018), in spatialized hydrology (Castaings et al., 2009; Jay-Allemand et al., 2020)) and for solver hybridization with neural networks (cf. framework proposed for learnable regionalization (Huynh et al., 2024b) and internal flux correction (Huynh et al., 2024a)
 45 in spatialized hydrology, enhanced and analyzed over a large sample in (Huynh et al., 2025)) model parameterization and structure learning. An important aspect is also to deliver carefully tested and documented code, user guides and datasets to ensure reproducibility of results and foster the diffusion of approaches and their evolution, taking advantage of other algorithms and advances from other scientific fields (e.g. other geophysical and environmental models, applied mathematics, signal processing, scientific computing).

50 The "resolution-complexity continuum" (Clark et al., 2017) has been explored over the past five decades through various modeling approaches, ranging from point-scale processes numerically integrated at larger scales to spatially lumped representations of system responses (Hrachowitz and Clark, 2017). Among the diverse hydrological models and their underlying hypotheses, components generally describe water storage and transfer (e.g. Fenicia et al. (2011)) through various combinations and parameterizations of vertical and lateral storage-flux operators. Several model comparison experiments have analyzed differences between various modeling approaches, evaluating performance in terms of streamflow modeling (Perrin et al., 2001; Reed et al., 2004; Duan et al., 2006; Orth et al., 2015) and internal states such as soil moisture (Orth et al., 2015; Bouaziz et al., 2021). Orth et al. (2015) concluded that "added complexity does not necessarily lead to improved performance of hydrologi-



cal models". Notably, parsimonious conceptual models, whether lumped or semi-lumped, have performed efficiently in large sample studies (e.g. GR model in Perrin et al. (2001), GRSD model in De Lavenne et al. (2019), GR and MORDOR models in Mathevet et al. (2020), FUSE models in Lane et al. (2019) and references therein). Large sample studies have also been undertaken with spatially distributed models among which VIC (Mizukami et al., 2017) with MPR regionalization (Samaniego et al., 2010), a gridded version of HBV applied with MPR like descriptors-to-parameters regressions on a global dataset (Beck et al., 2020), NHM (Towler et al., 2023) or Wflow (Aerts et al., 2022; van Verseveld et al., 2024). These large sample studies enable more general and statistically sound analyses of model performances (Andréassian et al., 2009; Gupta et al., 2014), addressing large-scale challenges with consistent methodologies across various scales and conditions.

All hydrological models are inherently conceptual and calibration or learning is generally required due to limitations and uncertainties in their structure, parameter representativity, data availability and initial and boundary conditions. These models are typically calibrated and validated using discharge time series at the catchment outlet(s) (Sebben et al., 2013). However, calibrating hydrological model parameters from sparse and integrative discharge data is a challenging inverse problem complicated by equifinality issues (Bertalanffy, 1968; Beven, 1993, 2001) especially for distributed models with a large number of cells and parameters ("curse of dimensionality"). Using spatially uniform parameters may not be the best way to exploit a spatially distributed model (under parameterization), while fully distributed parameters calibration, which requires a gradient based approach (Castaings et al., 2009; Jay-Allemand et al., 2020), is facing overparameterization. Therefore, a parameter regionalization approach using multilinear descriptors-to-parameters transfer functions has been proposed for distributed models (Beck et al., 2020). More recently, this approach has been advanced with regionalization neural networks (Huynh et al., 2024b) integrated into the differentiable spatialized `smash` model (Colleoni et al., 2022), which is the focus of the present article introducing a new numerical code and conducting original tests on a large sample of catchments with open source data. This approach also enables learning via cost functions based on hydrological signatures, which are obtained using automatic signal analysis algorithms applicable to large samples with `smash` (Huynh et al., 2023).

This article presents the computational framework `smash` dedicated to *Spatially distributed Modeling and ASsimulation for Hydrology*. The `smash` framework combines vertical and lateral flow operators, either process-based conceptual or hybrid with neural networks (allows learning regionalization relations between descriptors and parameters), and perform high dimensional optimization from multi-source data. It is based on an efficient and automatically differentiable Fortran solver enabling CPU parallel computing, that is interfaced in Python using `f90wrap` (Kermode, 2020; Jay-Allemand et al., 2022). This open-source `smash` code, in its version v1.0 (<https://github.com/DassHydro/smash>), is presented here in terms of mathematical formulation, numerical modeling approach and functionalities while full details can be found in our research articles from which this software stems (Colleoni et al., 2022; Huynh et al., 2023, 2024b) and in the online documentation (<https://smash.recover.inrae.fr>). Note that `smash` has also been developed for operational applications. It is the core solver of the French flash flood forecasting system (Piotte et al., 2020).

This article is organized as follows. Section 2 describes the `smash` forward model and the inverse algorithm. In section 3 we describe the `smash` build system framework, documentation and computational performance. Some applications of `smash` are demonstrated in section 4 using open-source datasets focusing on the contiguous United States (CONUS) and on a high-



resolution flash flood-prone case study in France. Section 5 illustrates other aspects of `smash` not presented in section 4, followed by conclusions in section 6.

95 2 Model and optimization algorithms description

The `smash` framework contains various hydrological model structures with varying vertical and lateral flow operators as well as spatialized routing schemes. It is designed to simulate discharge hydrographs and hydrological states at any spatial location within a gridded domain and it reproduces the hydrological response of contrasted catchments by taking advantage of spatially distributed meteorological forcings, physiographic data and hydrometric observations. Cost function gradient maps with respect to tunable parameters are a key feature of `smash` and can easily be combined to gradients of external operators such as a regionalization neural network (Huynh et al., 2024b) with chain rule in context of high dimensional optimization.

2.1 Forward model statement

Let $\Omega \subset \mathbb{R}^2$ denote a 2D spatial domain that can contain one to many gauges, with $x \in \Omega$ the spatial coordinate, $t \in]0, T]$ the physical time and \mathcal{D}_Ω a drainage plan over Ω . The spatially distributed rainfall-runoff model \mathcal{M} is a dynamic operator projecting the input fields of atmospheric forcings \mathcal{I} onto the fields of surface discharge Q , internal states \mathbf{h} , and internal fluxes \mathbf{q} , as expressed in Equation 1.

$$\mathbf{U}(x, t) = [Q, \mathbf{h}, \mathbf{q}](x, t) = \mathcal{M}(\mathcal{D}_\Omega; \mathcal{I}(x, t); [\boldsymbol{\theta}, \mathbf{h}_0](x)) \quad (1)$$

with $\mathbf{U}(x, t)$ the modeled state-flux variables, $\boldsymbol{\theta}$ and \mathbf{h}_0 the spatially distributed parameters and initial states of the hydrological model.

The spatially distributed rainfall-runoff model \mathcal{M} is obtained by partial composition (each operator taking various other input data and parameters) of the flow operators as follows:

$$\mathcal{M} = \mathcal{M}_{hy}(\cdot, \mathcal{M}_{rr}(\cdot, \mathcal{M}_{snw})) \quad (2)$$

Several operators structures are available in `smash` for composing a model:

– **Snow operator** \mathcal{M}_{snw} (optional): simulates melt flux $m_{lt}(x, t)$ feeding the hydrological operator in addition to rain.

- *zero*: no module
- *ssn*: degree-day module

– **Hydrological operator** \mathcal{M}_{rr} : simulation at pixel scale of elementary runoff $q_t(x, t)$ feeding the routing operator.

- *gr4*: GR-like module (Perrin et al., 2003; Mathevet, 2005)
- *gr5*: GR-like module (Le Moine, 2008; Ficchi et al., 2019)
- *grd*: GR-like module (Perrin et al., 2003; Jay-Allemand et al., 2020)



◦ *loieau*: GR-like module (Perrin et al., 2003; Folton and Arnaud, 2020)

◦ *vic3l*: VIC-like module adapted from (Liang et al., 1994)

– **Routing operator** \mathcal{M}_{hy} : runoff routing from pixels to pixel to obtain spatio-temporal discharge $Q(x, t)$.

◦ *lag0*: Instantaneous module

125 ◦ *lr*: Linear reservoir module

◦ *kW*: Kinematic wave module (Chow et al., 1998)

The operators chaining principle is schematized in Figure 1 with input data and internal states and fluxes, the operators available in `smash` are listed above and detailed in the documentation (https://smash.recover.inrae.fr/math_num_documentation/forward_structure.html).

130 Originally, a differentiable descriptors-to-parameters mapping ϕ can be used to constrain spatially distributed conceptual parameters $\theta(x)$ and initial states $h_0(x)$ from physical descriptors $D(x)$, for regionalization learning (Huynh et al., 2024b):

$$[\theta, h_0](x) = \phi(D(x), \rho), \forall x \in \Omega \quad (3)$$

with D the N_D -dimensional vector of physical descriptor maps covering the spatial domain Ω and ρ the vector of tunable regionalization parameters of the available mappings (written for θ only for brevity):

135 1. A set \mathcal{P} of multiple regression operators for each parameter of the forward hydrological model \mathcal{M} :

$$\theta_k(x, D, \rho_k) = s_k \left(\alpha_{k,0} + \sum_{d=1}^{N_D} \alpha_{k,d} D_d^{\beta_{k,d}}(x) \right), \forall k \in [1..N_\theta] \quad (4)$$

with $s_k(z) = l_k + (u_k - l_k) / (1 + e^{-z})$, $\forall z \in \mathbb{R}$ a transformation based on a sigmoid function with values in $]l_k, u_k[$ imposing constraints into the forward model such that $l_k < \theta_k(x) < u_k, \forall x \in \Omega$. The bounds l_k and u_k associated to each

140 conceptual parameter θ_k are spatially uniform. The regional parameter control vector to estimate in this case is: $\rho \equiv [(\rho_k)_{k=1}^{N_\theta}]^T \equiv \left[\left(\alpha_{k,0}, (\alpha_{k,d}, \beta_{k,d})_{d=1}^{N_D} \right)_{k=1}^{N_\theta} \right]^T$; a multiple linear regression mapping is obtained by imposing $\beta_{k,d} = 1$.

2. An ANN denoted \mathcal{N} , consisting of a multilayer perceptron, aimed at learning the descriptors-to-parameters mapping such that:

$$\theta(x, D, \rho) = \mathcal{N}(D(x), \mathbf{W}, \mathbf{b}), \forall x \in \Omega \quad (5)$$

where \mathbf{W} and \mathbf{b} are respectively weights and biases of the neural network composed of N_L dense layers. The architecture of the neural network and the forward propagation is detailed in Huynh et al. (2024b). Note that an output layer consisting of a scaling transformation is used to impose bound constraints as above. The regional control vector in this case is

$$\rho \equiv [\mathbf{W}, \mathbf{b}]^T \equiv [(\mathbf{W}_j, \mathbf{b}_j)_{j=1}^{N_L}]^T$$

Note that:



150

- The available mappings for ϕ are also implemented to predict initial state vector h_0 using physical descriptors fields that can include previous states and can be used for short range data assimilation (not studied here).
- By construction, the complete forward model \mathcal{M} is learnable in terms of parameters regionalization, through the regionalization mapping ϕ embedded into \mathcal{M} that is also differentiable, and its parameters ρ can be trained using cost gradient as explained after.

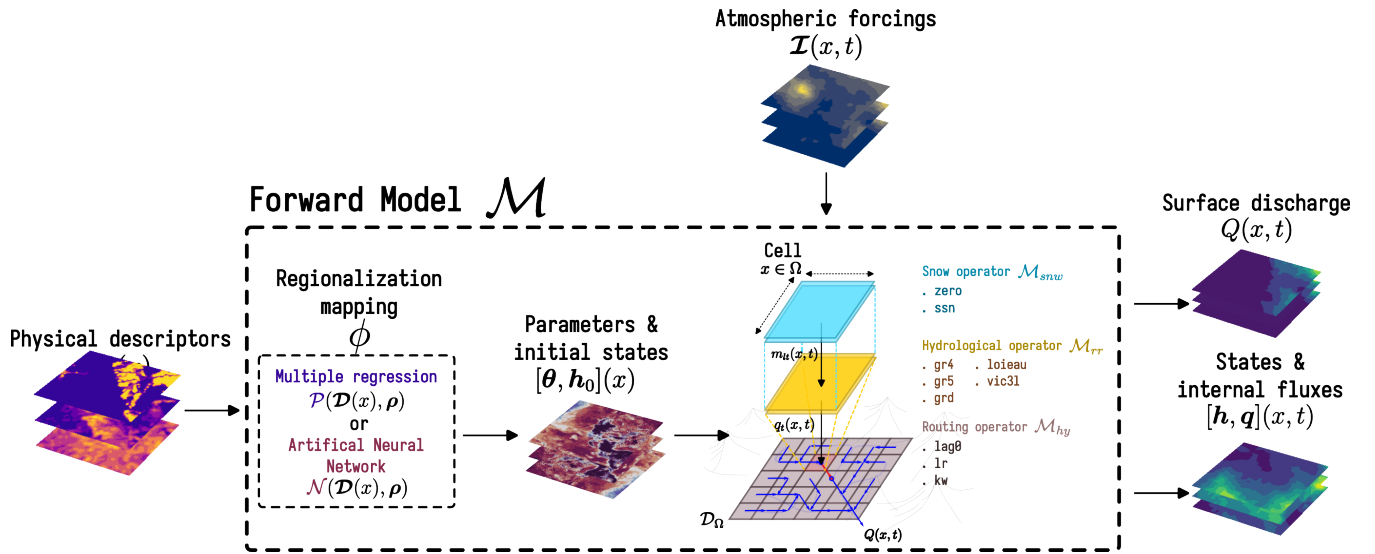


Figure 1. Flowchart of input data, operators chaining to obtain the forward differentiable model \mathcal{M} that includes a learnable regionalization mapping ϕ (Huynh et al., 2024b), and simulated states and fluxes. The forward model \mathcal{M} is obtained by partial composition (each operator taking various other input data and parameters) of the flow operators $\mathcal{M} = \mathcal{M}_{hy}(\cdot, \mathcal{M}_{rh}(\cdot, \mathcal{M}_{snow}(\cdot)))$.

2.2 Inverse algorithm

- 155 Given observed and simulated discharge times series $Q^* = (Q_{g=1..N_G}^*)^T$ and $Q = (Q_{g=1..N_G})^T$ with N_G the number of gauges over the study domain Ω , the model misfit to multi-site observations is measured through a cost function J that writes as

$$J(Q^*, Q) = \sum_{g=1}^{N_G} w_g j_g(Q_g^*, Q_g) + j_{reg}, \quad (6)$$

- 160 with w_g the weight associated to the cost function j_g at each gauge g , where $\sum_{g=1}^{N_g} w_g = 1$. This multi-gauge observation cost function is also used for mono-gauge calibration with $N_G = 1$. A regularization term j_{reg} can be considered for ill-posed inverse problems (cf. Jay-Allemand et al. (2020, 2024)).



The gauge cost function is defined as

$$j_g(Q_g^*, Q_g) = \sum_{c=1}^{N_C} w_c j_c(Q_g^*, Q_g), \quad (7)$$

with j_c being respectively based on any efficiency metric (NSE , KGE (Gupta et al., 2009), etc) or a signature-based cost
 165 function including N_C continuous and event-based components (Huynh et al., 2023) and w_c their relative weights. For multi-
 score calibration strategy using continuous NSE and event-based flood signatures see Huynh et al. (2023).

The global cost function J is defined as a convex and differentiable function, involving the response of the forward model
 \mathcal{M} through its output Q , and consequently depends on the model parameters θ , hence on the parameters ρ of the regional
 mapping ϕ when used (Eq. 3).

170 Therefore, the variational data assimilation (VDA) optimization problem formulates as in Equation 8:

$$\hat{\rho} = \arg \min_{\rho} J(Q^*, \mathcal{M}(\cdot, \phi(\cdot, \rho))) \quad (8)$$

This high-dimensional inverse problem can be tackled with gradient-based optimization algorithms. A limited-memory quasi-
 Newton approach, such as L-BFGS-B (Zhu et al., 1997), is suitable for smooth objective functions, while an adaptive learning
 rate approach, exemplified by Adam (Kingma and Ba, 2014), is effective for non-smooth objective functions. These approaches
 175 necessitate obtaining the gradient $\nabla_{\rho} J$ of the cost function with respect to the tunable control parameter ρ obtained by solving
 the adjoint $D_{\rho} \mathcal{M}$ of the forward model \mathcal{M} . The adjoint model is obtained by automatic differentiation using the Tapenade
 engine (Hascoet and Pascual, 2013). The complete forward model and variational data assimilation process are illustrated in
 Figure 2.

3 Computational software and performance

180 In this section, we focus on code architecture, documentation and computational performance. `smash` is based on a computa-
 tionally efficient Fortran core enabling parallel computations over large domains with `OpenMP` (Dagum and Menon, 1998), and
 that is automatically differentiable with the Tapenade engine (Hascoet and Pascual, 2013) to generate the numerical adjoint
 model. It is interfaced in Python using `f90wrap` (Kermode, 2020) to provide a user-friendly and versatile interface for quick
 learning and efficient development, as well as to directly make accessible the wealth of Python modules and libraries (Tab. 1)
 185 developed by a large and active community (Data pre/post-Processing, Geographic Information System, Deep Learning, etc).

3.1 From sources to ready-to-use Python library

`smash` contains a Python core for all the user interface functions, both pre- and post-processing, and a Fortran core (with a
 few C files) for high-performance numerical computations. In order to produce a Python library, including binary files, that
 can be installed directly from the package manager, `PyPI`, several steps are necessary. The first step is to generate the Fortran
 190 adjoint file from the Fortran sources. This is done via Tapenade automatic differentiation engine (Hascoet and Pascual,
 2013), which requires the use of Java. Next, the Fortran code is wrapped for use in Python. `f90wrap` (Kermode, 2020) builds

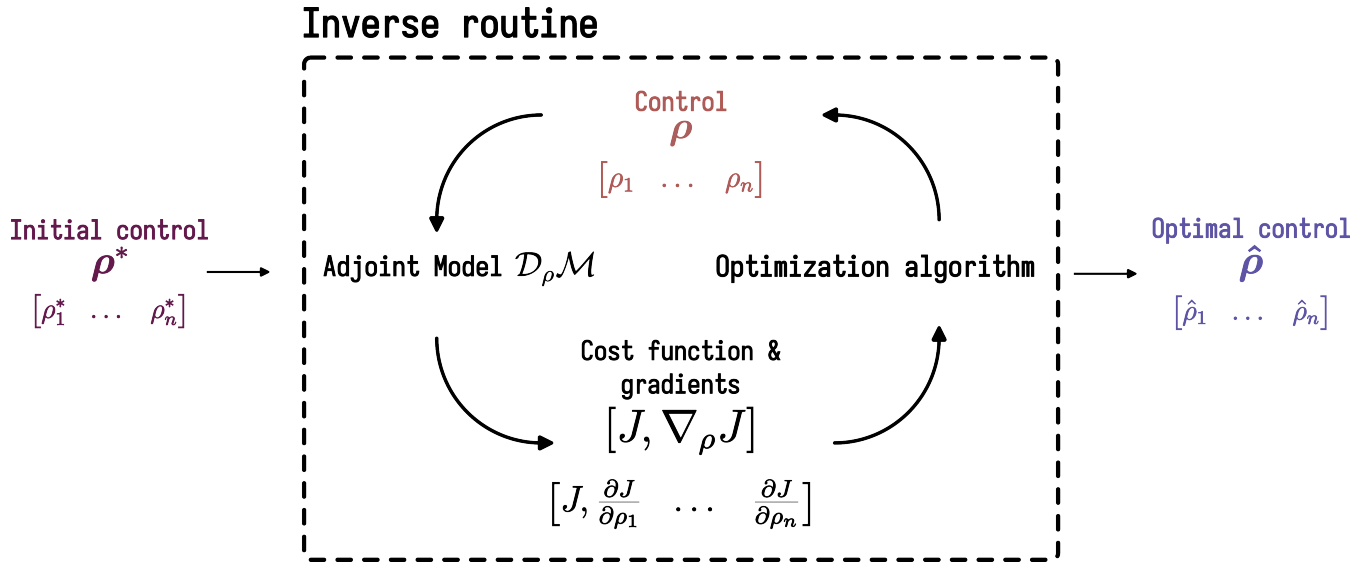


Figure 2. Flowchart of the inverse algorithm that uses $\nabla_{\rho} J$ the cost gradient with respect to the tunable control parameter ρ obtained by solving the adjoint $D_{\rho} \mathcal{M}$ of the forward model \mathcal{M} (adapted from VDA course Monnier (2024)).

Table 1. External Python libraries used by `smash`.

Library	Website	Reference	Description
NumPy	https://numpy.org	Harris et al. (2020)	Numerical computing
SciPy	https://scipy.org	Virtanen et al. (2020)	
pandas	https://pandas.pydata.org	pandas development team (2020)	Data analysis and manipulation tool
f90wrap	https://github.com/jameskermode/f90wrap	Kermode (2020)	Fortran to Python interface generator
Rasterio	https://rasterio.readthedocs.io/en/stable		Input/output
h5py	https://docs.h5py.org/en/stable		

on the capabilities of the popular `F2PY` utility by generating a simpler Fortran interface to the original Fortran sources which is then suitable for wrapping with `F2PY`, together with a higher-level Pythonic wrapper that makes the existence of an additional



195 layer transparent to the final user. The entire build system (except for the generation of the adjoint file, which is external for debugging reasons) is handled by `meson`, a multi-platform, multi-language open-source build system that allows us to generate `smash` binaries on Linux, macOS and Windows quite easily (Fig. 3).

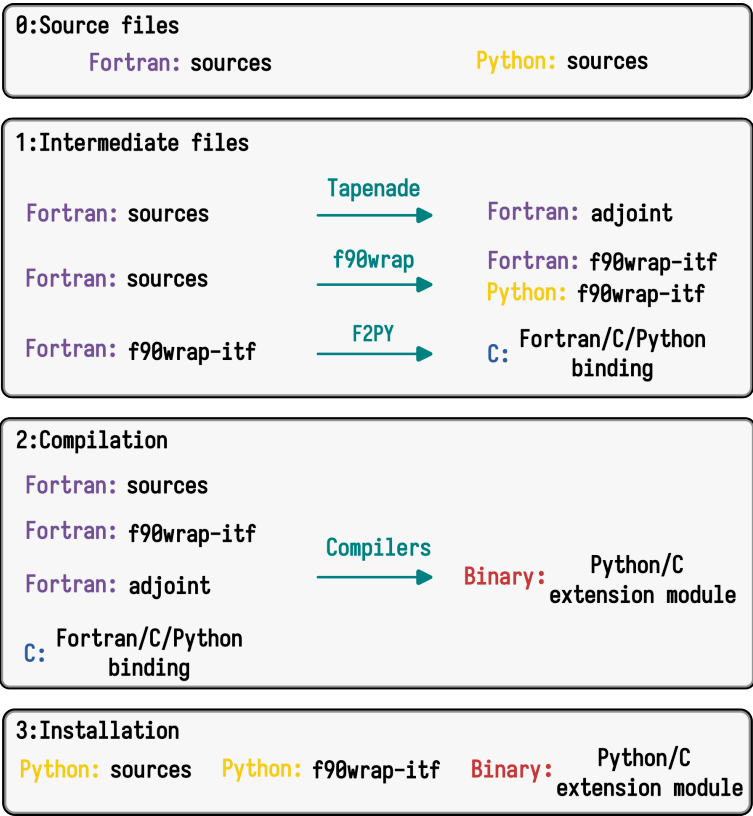


Figure 3. The `smash` build system framework. It starts with source files written in Fortran and Python (0). In the intermediate step (1), Fortran sources are processed by `Tapenade` to generate the adjoint code, and wrapped using `f90wrap` to create Python interfaces (`f90wrap-itf`). The `F2PY` tool is then used to generate a Fortran/C/Python binding from the wrapped interfaces. During the compilation step (2), the original Fortran sources, adjoint code, and `f90wrap-itf` are compiled with appropriate compilers to produce a binary Python/C extension module. Finally, in the installation step (3), the Python module is assembled, combining the original Python sources with the `f90wrap-itf` and the compiled binary Python/C extension module, making the high-performance Fortran code accessible from Python.

3.2 Documentation

The `smash` online documentation (Fig. 4) is divided into four main sections:

- Getting Started (https://smash.recover.inrae.fr/getting_started)

200 This section describes how to install `smash` from the Python package index `PyPI`.



- User Guide (https://smash.recover.inrae.fr/user_guide)

This section provides step-by-step examples (and scripts) from basic (simulation run) to complex (regionalization) applications of `smash` as well as input data conventions.

- API Reference (https://smash.recover.inrae.fr/api_reference)

205 This section details the different modules and the application programming interface. Modules are documented using the NumPy-style Python docstring.

- Math / Num Documentation (https://smash.recover.inrae.fr/math_num_documentation)

This last section details the conceptual and mathematical basis of the forward and inverse modeling problems, their numerical resolution along with optimization and estimation algorithms.

210 The whole documentation is implemented using `Sphinx` to automatically compile and update an online version.

3.3 Computational performance

In this section, we compare the performance of `smash` in terms of computation time and memory usage between direct and inverse runs (an inverse run is equivalent to a single call to the adjoint model $D_p \mathcal{M}$ here). The aim is to highlight the resources required to run `smash` on configurations similar to real cases. We compare `smash` over 3 zones: Sardinia, Great
215 Britain/Ireland and North America at a spatial resolution of 1'30" ($\sim 3\text{km} \times 3\text{km}$) over a period of 1 year, randomly chosen, at a daily time step. These 3 zones were chosen simply to provide 3 zones of variable surface area (Fig. 5). In addition to the 3 zones, with `smash` enabling different assemblies of operators, two structures are compared, `s1` and `s2`, representing respectively the simplest (\mathcal{M}_{snw} : *zero*, \mathcal{M}_{rr} : *grd* and \mathcal{M}_{hy} : *lag0*) and the most complex (\mathcal{M}_{snw} : *ssn*, \mathcal{M}_{rr} : *vic3l* and \mathcal{M}_{hy} : *kw*) structure in terms of number of operations per cell. All the simulations (1 year of simulation at daily time step) were run
220 on a server with AMD EPYC 7643 CPUs (Annexe B1) and 255 GB of RAM.

The range of computation times across all simulations (Fig. 6) varies from approximately 0.1 second for a direct run with 8 CPUs on the Sardinia region using the `s1` structure to just over an hour for an inverse run with 1 CPU on the North America region using the `s2` structure. Systematically, regardless of the region, number of CPUs, or type of run, the difference in computation time between the `s1` and `s2` structures is about a factor of 2. Regarding the differences between a direct run and
225 an inverse run, the computation time factor varies depending on the number of CPUs, ranging from a factor of 12 for 1 CPU to a factor of 6 for 16 CPUs. This difference highlights better CPU scaling for the inverse run, with a speedup of around 4 for a direct run and 7 for an inverse run with 16 CPUs. It is worth noting that in the case of the Sardinia region, which has the fewest grid cells, CPU scaling is poor compared to the other two regions, even reaching the limit where CPU overhead increases the computation time. Since the time-stepping loop and the routing scheme cannot be parallelized, it results in a non-linear scaling
230 but it remains interesting as it significantly reduces computation time.

About memory usage (Tab. 2), values range from 0.17 GB for a direct run on the Sardinia region with the `s1` structure to 27 GB for an inverse run on the North America region with the `s2` structure. Systematically, memory usage is higher in an inverse

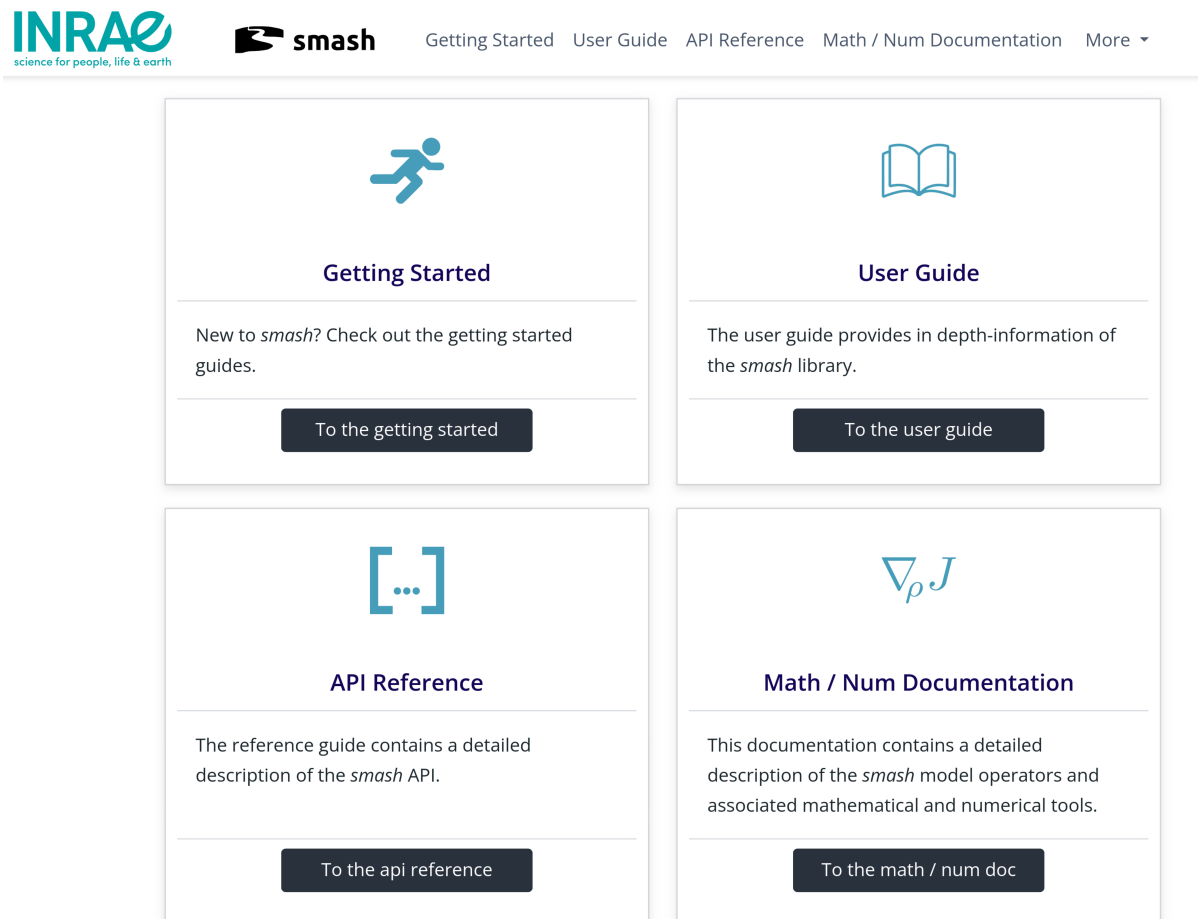


Figure 4. *smash* documentation home page accessible at <https://smash.recover.inrae.fr>.

run than in a direct run and scales with the size of the domain. The main contributor to memory usage in an inverse run is the forward sweep, which includes a time-stepping loop where iteration n depends on the results of previous iterations. The memory allocation during the forward sweep is freed during the backward sweep, but it still results in a significant memory peak. This memory peak has been considerably reduced in the *smash* version presented here by including checkpoints within the time-stepping loop. These checkpoints allow to alternate between forward and backward sweeps, leading to much smaller memory peaks compared to a single sweep. The downside of using checkpoints is the increase in computation time, but this was considered less significant compared to the memory savings (see Hascoet and Pascual (2013) for further details about forward/backward sweep and checkpointing).

In conclusion, these computation times and memory usage demonstrate the feasibility of the model for large-scale applications. The critical point is parameters estimation. In the case of parameters estimation using a gradient-based optimizer, one or more inverse runs are evaluated at each iteration, significantly multiplying the total computation time. As an example,



Huynh et al. (2024b) performed a calibration at a spatial resolution of 1km over a domain of more than 20,000 cells, and at a
 245 temporal resolution of one hour over a period of 4 years. The calibration required 350 calls to the adjoint model, resulting in a
 computation time of around 180 hours. Currently, memory usage in an inverse run is less of a limiting factor than computation
 time for large-domain applications. Thus, further improving computation time is a priority to expand the model's application
 to finer spatial and temporal scales.

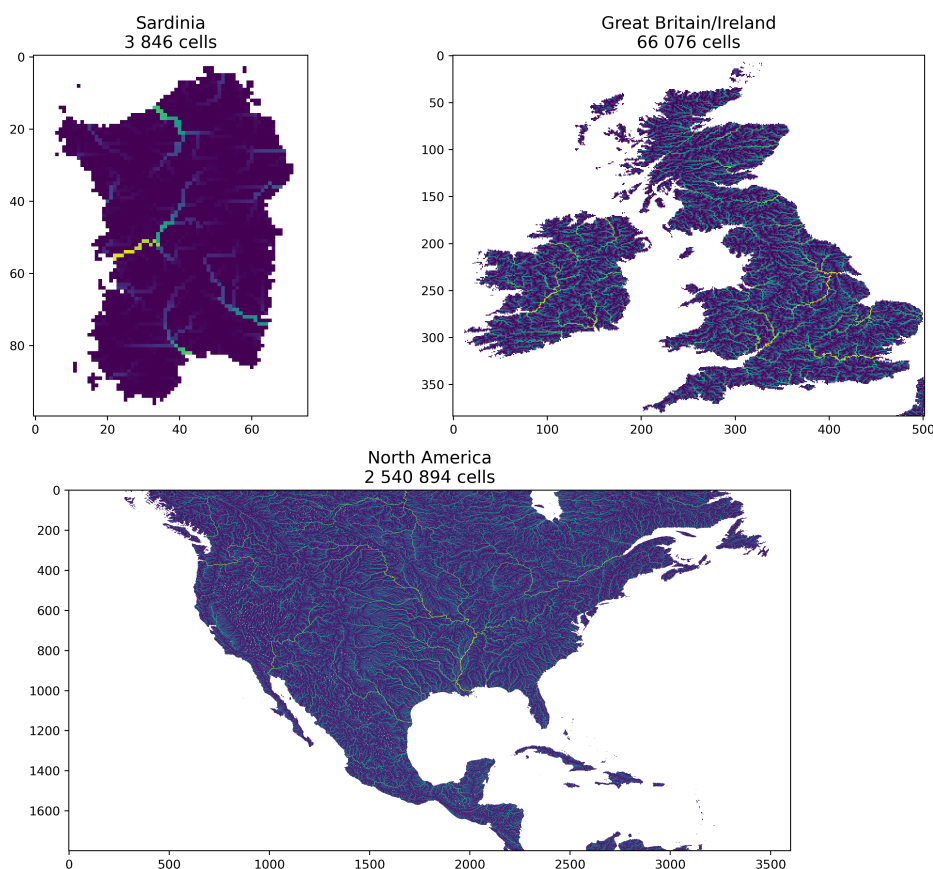


Figure 5. Spatial representations of the three different geographical regions used in the performance benchmarks.

4 Applications

250 4.1 Numerical experiments presented

Main functionalities and operators of `smash` are illustrated on open-source global datasets over contiguous United States
 (CONUS) (Tab. 3, Fig. 7) and on a higher resolution open-source regional dataset in France (Tab. 4, Fig. 7). Models on

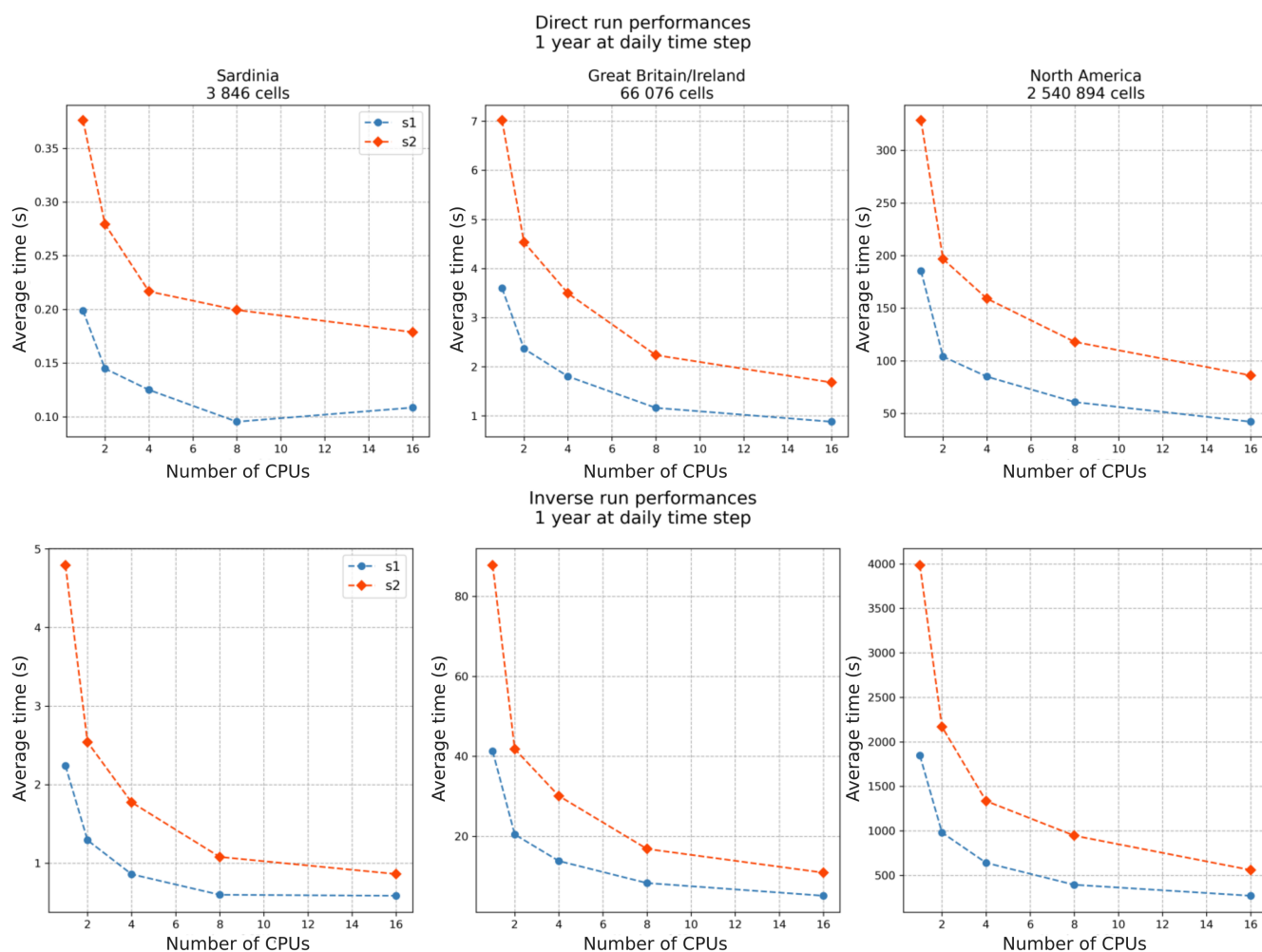


Figure 6. Benchmarking results for both direct (top row) and inverse (bottom row) run simulations over a period of 1 year at daily time step, using varying numbers of CPUs (from 1 to 16). Each plot corresponds to a different geographical region: Sardinia, Great Britain/Ireland and North America from left to right.



Table 2. Memory usage in Gigabyte (GB) for both direct and inverse run simulations over a period of 1 year at daily time step.

Zone	Structure	Memory Usage (GB)	
		Direct	Inverse
Sardinia	s1	0.17	0.18
	s2	0.18	0.20
Great Britain/Ireland	s1	0.37	0.46
	s2	0.52	0.86
North America	s1	7.64	11.27
	s2	12.7	26.68

CONUS will be at a spatial resolution of 1'30" ($\sim 3\text{km} \times 3\text{km}$) and daily time step while higher resolution models will be setup on the French case at 500-m spatial resolution and hourly time step. The numerical results presented are:

- 255
- Split-sample temporal cross-validation of different model structures combinations over CONUS (Sect. 4.2)
 - Regionalization over CONUS (Sect. 4.3)
 - High-resolution regionalization over the Aude river in France (Sect. 4.4).

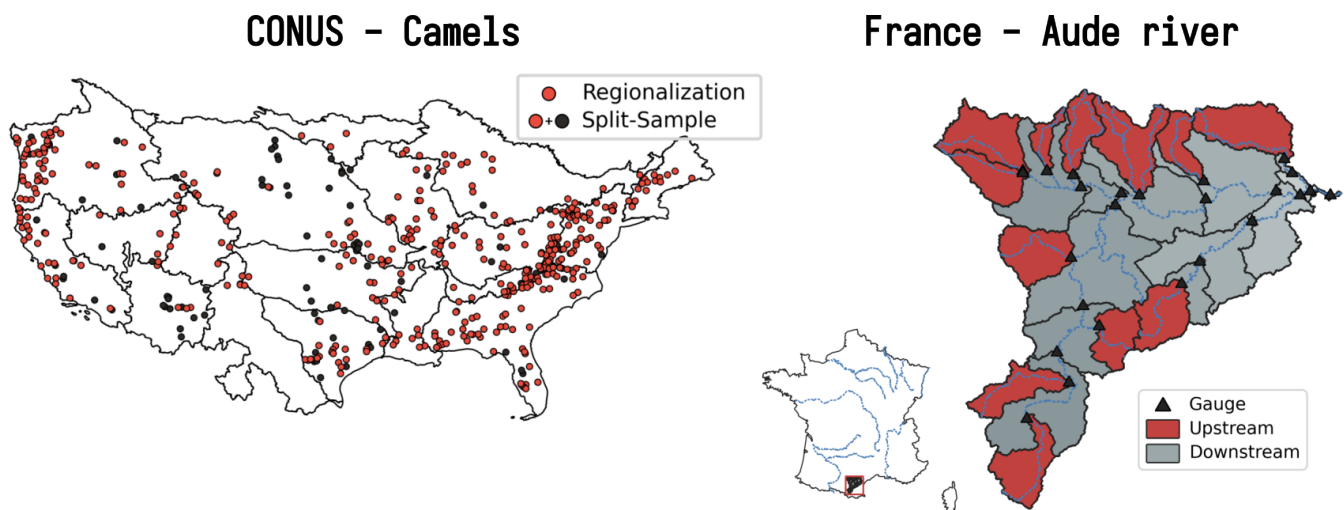


Figure 7. Location of the catchments for the CONUS (left) and France (right) applications. For the split-sample test over CONUS, all the 482 catchments from the CAMELS dataset (Addor et al., 2017) are used (orange and black circles) whereas for the regionalization a subset of 398 catchments is used (only orange circles), removing catchments whose performance are less than 0.75 *KGE* from local calibration. For the France application over the Aude river, a set of 25 sub-catchments is used for regionalization with 12 upstream catchments (red shaded regions) and 13 downstream catchments (gray shaded regions).



Table 3. Model input data from open-source databases available worldwide used over CONUS: atmospheric forcings $\mathcal{I} = \{P, N, E, T\}$, flow direction map \mathcal{D}_Ω , physical descriptors $D = \{d_1, \dots, d_6\}$ for regionalization based on Beck et al. (2020) study and discharge time series Q^* . The liquid and solid precipitation, P and N , derive from the Multi-Source Weighted-Ensemble Precipitation (MSWEP) (Beck et al., 2019) divided into liquid and solid parts using a parametric S-shaped curve (Garavaglia et al., 2017) and disaggregated from 0.1° to 0.025° . The temperature and potential evapotranspiration, T and E , derive from ERA5 (Hersbach et al., 2020) disaggregated from 0.25° to 0.025° , using the Oudin formula (Oudin et al., 2005) to obtain the potential evapotranspiration. The flow direction, \mathcal{D}_Ω , from MERIT Hydro IHU (Eilander et al., 2021) was upscaled from 0.008° to 0.025° using `pyflwdir` (Eilander, 2023). The topographic slope, d_1 , derives from MERIT DEM (Yamazaki et al., 2017) upscaled from 0.008° to 0.025° using `gdaldem slope`. The sand and clay content, d_2 and d_3 , from SoilGrids (Hengl et al., 2017) were upscaled and reprojected from 250m to 0.025° . The meteo-climatic data, d_4 , d_5 and d_6 derive from P and E . The discharge time series, Q^* , comes from Caravan-CAMELS (Kratzert et al., 2023; Addor et al., 2017).

Notation	Type	Description	Unit	Source
P	Atmospheric forcing	Liquid precipitation	(mm/day)	MSWEP (Beck et al., 2019)
N	Atmospheric forcing	Solid precipitation	(mm/day)	MSWEP (Beck et al., 2019)
E	Atmospheric forcing	Potential evapotranspiration using Oudin formula (Oudin et al., 2005)	(mm/day)	ERA5 temperature (Hersbach et al., 2020)
T	Atmospheric forcing	Temperature	(°C)	ERA5 temperature (Hersbach et al., 2020)
\mathcal{D}_Ω	Topography	Flow direction	(–)	MERIT Hydro IHU (Eilander et al., 2021)
d_1 (slope)	Topography	Topographic slope	(°)	MERIT (Yamazaki et al., 2017)
d_2 (sand)	Soil	Sand content, averaged over all layers	(g/kg)	SoilGrids (Hengl et al., 2017)
d_3 (clay)	Soil	Clay content, averaged over all layers	(g/kg)	SoilGrids (Hengl et al., 2017)
d_4 (prcp)	Meteo-Climatic	Mean annual precipitation	(mm/yr)	MSWEP (Beck et al., 2019)
d_5 (pet)	Meteo-Climatic	Mean annual potential evapotranspiration using Oudin (Oudin et al., 2005)	(mm/yr)	ERA5 temperature (Hersbach et al., 2020)
d_6 (hi)	Meteo-Climatic	Mean annual humidity index (ratio of precipitation to potential evapotranspiration)	(–)	MSWEP (Beck et al., 2019), ERA5 temperature (Hersbach et al., 2020)
Q^*	Hydrometric	Discharge time series	(m ³ /s)	Caravan-CAMELS (Kratzert et al., 2023; Addor et al., 2017)



Table 4. Model input data from national open-source databases used over the Aude river in France: atmospheric forcings $\mathcal{I} = \{P, E\}$, flow direction map \mathcal{D}_Ω , physical descriptors $D = \{d_1, \dots, d_7\}$ for regionalization and discharge time series Q^* . The liquid precipitation, P , comes from the ANTILOPE J+1 Météo-France product (Champeaux et al., 2009), a radar-gauge reanalysis disaggregated from 1km to 500m. The potential evapotranspiration, E , derives from the SAFRAN Météo-France temperature (Quintana-Seguí et al., 2008; Vidal et al., 2010) disaggregated from 8km to 500m, using the Oudin formula (Oudin et al., 2005) to obtain a daily interannual potential evapotranspiration. The flow direction, \mathcal{D}_Ω , comes from HydroDem (Leblois and Sauquet, 1999). The land cover data, d_1 , d_2 , d_3 and d_4 derive from CORINE Land Cover 2018 (doi.org) rasterized at 50m and upscaled to 500m using the average resampling method. The topographic slope, d_5 , derives from HydroDem DEM (Leblois and Sauquet, 1999) using `gdaldem slope`. The drainage density, d_6 comes from (Organde et al., 2013) representing the number of cells crossed by a river. The percentage of karst, d_7 , comes from BDLISA (<https://bdlisa.eaufrance.fr/>) rasterized at 50m and upscaled to 500m using the average resampling method. The discharge time series, Q^* , comes from HydroPortail Service Central Vigicrues (<https://hydro.eaufrance.fr/>).

Notation	Type	Description	Unit	Source
P	Atmospheric forcing	Liquid precipitation	(mm/h)	Antilope J+1 from Météo-France (Champeaux et al., 2009)
E	Atmospheric forcing	Potential evapotranspiration using the Oudin formula (Oudin et al., 2005)	(mm/h)	SAFRAN temperature from Météo-France (Quintana-Seguí et al., 2008; Vidal et al., 2010)
\mathcal{D}_Ω	Topography	Flow direction	(—)	HydroDem (Leblois and Sauquet, 1999)
d_1 (artif)	Land cover	Artificial cover rate	(—)	CORINE Land Cover 2018 (doi.org)
d_2 (forest)	Land cover	Forest cover rate	(—)	CORINE Land Cover 2018 (doi.org)
d_3 (veg)	Land cover	Vegetation cover rate	(—)	CORINE Land Cover 2018 (doi.org)
d_4 (ow)	Land cover	Open water cover rate	(—)	CORINE Land Cover 2018 (doi.org)
d_5 (slope)	Topography	Topographic slope	(°)	HydroDem (Leblois and Sauquet, 1999)
d_6 (ddr)	Topography	Drainage density	(—)	(Organde et al., 2013)
d_7 (karst)	Hydrogeology	Percentage of karst	(%)	BDLISA (https://bdlisa.eaufrance.fr/)
Q^*	Hydrometric	Discharge time series	(m ³ /s)	HydroPortail SCHAPI (https://hydro.eaufrance.fr/)

4.2 CONUS - CAMELS - Split-sample temporal cross-validation

4.2.1 Numerical experiment settings

260 A set of 482 catchments (Fig. 7) is modeled with the following experimental design:

- A set of hydrological models is considered, including 4 GR-like structures (Perrin et al., 2003) (\mathcal{M}_{rr} : *gr4*, *gr5*, *grd*, *loieau*) and one VIC-like structure (Liang et al., 1994) (\mathcal{M}_{rr} : *vic3l*). The way in which these models are integrated into *smash*, that differs from the original models, is described in the documentation (https://smash.recover.inrae.fr/math_



[num_documentation/forward_structure.html](#)) in the forward structure section. For each hydrological model, the same snow module ($\mathcal{M}_{snw}: ssn$) and routing module ($\mathcal{M}_{hy}: kw$) are used.

- A split-sample temporal validation procedure (Klemeš, 1983) is set up splitting the time window covered by hydrometric data into two complementary subsets over sub-periods of 7 years: $p1$ (from 1 August 2000 to 31 July 2007) and $p2$ (from 1 August 2007 to 31 July 2014) are both used for calibration and validation. For each period, 10 years are used as model "warm-up".
- 2 calibration mappings on each catchment are tested:
 - Uniform: spatially uniform parameters
 - Distributed: spatially distributed parameters
- The use of a single-gauge cost function based on the KGE ($J = 1 - KGE$)

4.2.2 Results

The performance of the models resulting from the spatially uniform or distributed calibration is evaluated using the Kling-Gupta Efficiency (KGE) for both the calibration and the validation on period $p2$ only for brevity in this software article (Fig. 8). Overall performance is satisfactory, with a median between 0.8 and 0.87 for KGE over the calibration period and between 0.72 and 0.78 for KGE over the validation period. With regard to the calibration method, for any model, calibration and validation performances are better with a spatially distributed calibration. This is an expected result for the calibration period, given that spatially distributed calibration is over-parameterised and offers the maximum level of flexibility in the search for the optimal set of parameters, unlike spatially uniform calibration, which is under-parameterised, imposing a single parameter set for each catchment. However, despite this over-parametrisation with calibration of spatially distributed parameters, which can lead to over-fitting over the calibration period, the models offer good performance in temporal validation. The differences between the structures are mainly explained by (i) the varying levels of model complexity, 2 parameters for the *grd* model and 4 for the *gr5* model, and (ii) the expert knowledge of the different models, which influences, among other things, the choice of initial values, bounds and parameters to be optimised. The *smash* historical development based on the GR-like models led to a much more substantial expert knowledge than for the VIC-like model recently implemented.

Concerning the spatial distribution of KGE values (Fig. 9), the results for the *gr4* hydrological model after a spatially distributed calibration show that the best performances are located over the east and west sides of CONUS while worst performances are located over the Great Plains area. This spatial pattern of hydrological model performance has also been obtained in other studies (Newman et al., 2015; Beck et al., 2016; Mizukami et al., 2017).

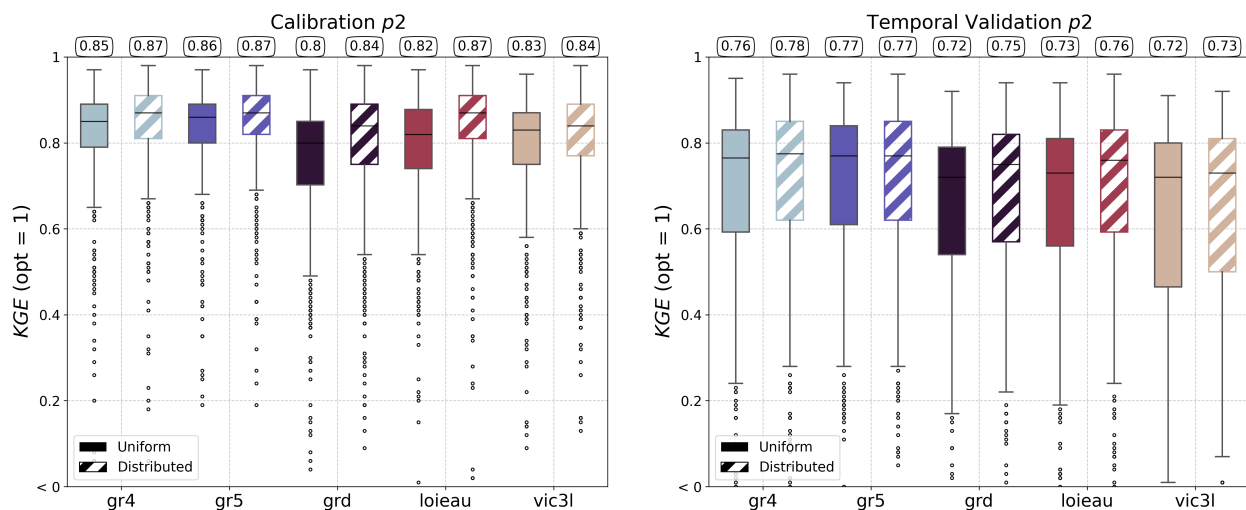


Figure 8. Comparison of the Kling-Gupta Efficiency (KGE) performance of different *smash* hydrological models under spatially uniform and distributed calibration. The models evaluated include *gr4*, *gr5*, *grd*, *loieau*, and *vic3l*. The left panels show results for the calibration, while the right panels display results for temporal validation on period $p2$. For each model, results are shown for spatially uniform (solid boxes) and spatially distributed (hatched boxes) calibrations with the median value highlighted at the top of the boxplot.

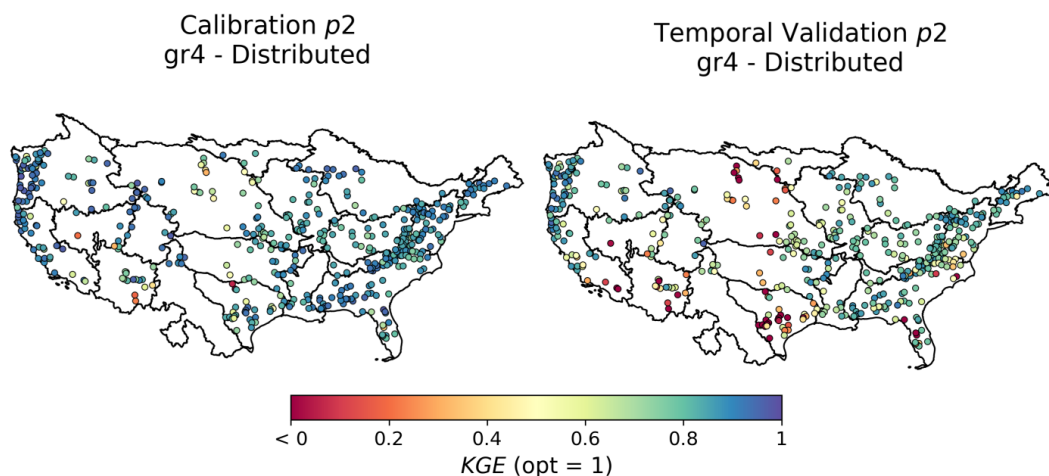


Figure 9. Spatial distribution of the Kling-Gupta Efficiency (KGE) scores across different catchments for the *gr4* model under local calibration with spatially distributed parameters. The left map shows KGE scores during the calibration period while the right map shows results for temporal validation, using the $p2$ period.



4.3 CONUS - CAMELS - Regionalization

4.3.1 Numerical experiment settings

A set of 398 catchments (Fig. 7) from the CAMELS dataset (Addor et al., 2017) is evaluated in a regionalization context at a
 295 spatial resolution of 1'30" and at a daily time step using worldwide databases (Tab. 3). The experimental design is as follows:

- Selection of a subset of catchments from Section 4.2, eliminating catchments where $KGE < 0.75$ from local calibration. This selection is made in order to avoid introducing catchments whose performance could greatly degrade the calibration metric in a multi-gauge context.
- One hydrological model is considered, identical to the *gr4* model in Section 4.2 with the same snow and routing module
 300 ($\mathcal{M}_{snw}: snn, \mathcal{M}_{rr}: gr4, \mathcal{M}_{hy}: kw$)
- A spatio-temporal validation procedure is set up by:
 - splitting the time window covered by hydrometric data into two complementary subsets over sub-periods of 7 years: $p1$ (from 1 August 2000 to 31 July 2007) and $p2$ (from 1 August 2007 to 31 July 2014), with $p1$ used as calibration period and $p2$ as validation period. For each period, 10 years are used as model "warm-up".
 - randomly splitting the catchment set into 4 groups, calibrating on 3 of the groups, with the 4th group held out and
 305 used for validation, then rotating such that each group is used for validation once.
- 3 calibration mappings across the whole CONUS are tested:
 - Uniform: spatially uniform parameters
 - Multi-Linear: a multiple linear regression is used as transfer function from descriptors to spatialized parameters
 - ANN: a multi-layer perceptron composed of 3 hidden layers is used as a transfer function from descriptors to
 310 spatialized parameters
- The use of a multi-gauge cost function based on the average KGE of the calibrated catchments ($J = \frac{1}{N_G} \sum^{N_G} 1 - KGE$)
- A final calibration over the total period $p1 + p2$ including all gauges with the ANN mapping and the same multi-gauge
 315 cost function to analyze the output model parameters and their correlations with input descriptors.

4.3.2 Results

The regional calibration over CAMELS dataset was performed on 4 groups of randomly selected catchments as explained above. The performances in spatial and/or temporal validation are shown in Figure 10 and detailed by catchment groups in Table A1 for the ANN mapping, which is the best performer. In spatio-temporal validation, the most challenging extrapolation



case, a uniform mapping leads to a median KGE of 0.5 while the two regionalization methods result in KGE of 0.61 or 0.63, respectively for Multi-Linear and ANN mapping. These fairly good performances, obtained with a relatively simple setup in terms of descriptors and cost function in particular, are comparable with regionalization works in the literature (Mizukami et al., 2019; Beck et al., 2020; Feng et al., 2024). In a similar way to the previous section (Sect. 4.2), the worst performances are located in the Great Plains but also, more clearly than in the local calibrations, in the western part of the country.

Following the evaluation of performance in spatio-temporal validation, a regional calibration with the ANN mapping over the period including $p1$ and $p2$ and with all gauges is carried out. This calibration enables us to analyze the correlations between the physiographic descriptors and the parameters obtained (Fig. 11), in a more robust way than with the various spatio-temporal validation groups. The correlation matrix highlights significant linear correlations, notably between the melt coefficient (k_{melt}) and the topographical slope (d_1), the size of the production reservoir (c_p) and the mean annual rainfall (d_4), as well as the moisture content (d_6) and the routing parameters (a_{kw} , b_{kw}) with the same moisture content (d_6). Conversely, the exchange parameter (k_{exc}), a parameter directly affecting the model's mass balance in a non-conservative way, shows almost no linear correlation with the descriptors and is almost spatially uniform over the whole domain around the value of 0. While a detailed regionalization study on CAMELS datasets using our original adjoint-based algorithms is beyond the scope of this software article, the achieved performance across this large sample already showcases the algorithm's potential for global applicability. It also demonstrates the algorithm's effectiveness in enforcing spatially distributed hydrologic model constraints at the pixel scale, leading to seamless parameter maps at a reasonable computational cost.

Finally, leveraging the fully distributed nature of `smash`, regional streamflow maps can be generated. An example is shown in Figure 12, which illustrates the dynamics of Hurricane Katrina over a 6-day period from August 27 to September 1, 2005. Notably, the routing model used in this exercise, the kinematic wave, was applied uniformly across the entire domain, including areas outside its validity range, such as downstream of major rivers on flat topography. Further work focuses on enriching `smash` with hydraulic models, starting with 1D and 2D non-inertial shallow water models for numerical implementation simplicity. Additionally, physics-based differential equations for hydrologic water balance at the pixel scale will be incorporated. Hybrid physics-AI formulations, which embed neural networks capable of learning parametrization and potentially uncertain model operators from data, can be explored thanks to the differentiable nature of the models within `smash`.

4.4 France - Aude river - High-resolution regionalization

4.4.1 Numerical experiment settings

A set of 35 catchments (Fig. 7) over the Aude river in France (Addor et al., 2017) is evaluated in a regionalization context at a spatial resolution of 500m and at a hourly time step using national databases (Tab. 4). The experimental design is as follows:

- One hydrological model is considered, identical to the *gr4* model in Section 4.2 with the same routing module but without any snow modeling given the limited impact of snow in this Mediterranean basin (\mathcal{M}_{snow} : zero, \mathcal{M}_{rr} : *gr4*, \mathcal{M}_{hy} : *kw*)
- A spatio-temporal validation procedure is set up by:

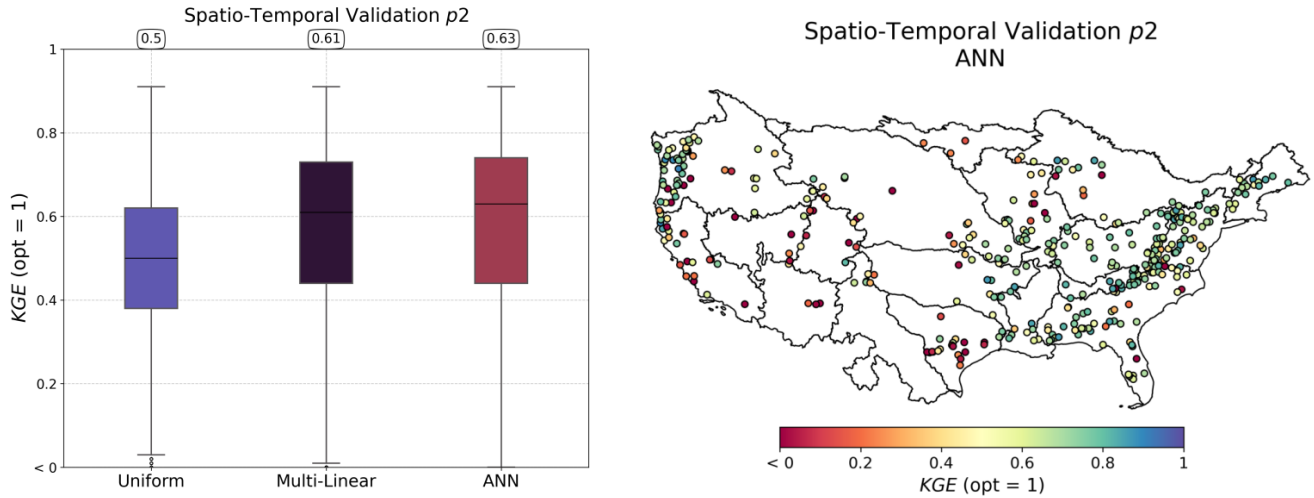


Figure 10. Spatio-temporal validation performance over period p_2 . The boxplots on the left panel represent the distribution of Kling-Gupta Efficiency (KGE) scores for three calibration methods: Uniform, Multi-Linear, and Artificial Neural Network (ANN). Median values are displayed at the top of each boxplot. The map on the right illustrates the spatial distribution of the KGE values for the ANN mapping across different catchments.

- splitting the time window covered by hydrometric data into two complementary subsets over sub-periods of 4 years: p_1 (from 1 August 2015 to 31 July 2019) and p_2 (from 1 August 2019 to 31 July 2023), with p_1 used as calibration period and p_2 as validation period. For each period, 1 year is used as model "warm-up".

355

- splitting the catchment set into 2 groups, upstream and downstream, calibrating on the upstream group and validating on the downstream group.

– 3 calibration mappings across the whole Aude river are tested:

- Uniform: spatially uniform parameters
- Multi-Linear: a multiple linear regression is used as the transfer function from descriptors to spatialized parameters
- ANN: a multi-layer perceptron composed of 3 hidden layers is used as the transfer function from descriptors to spatialized parameters

360

– The use of a multi-gauge cost function based on the average NSE of the calibrated catchments ($J = \frac{1}{N_G} \sum^{N_G} (1 - NSE)$).

4.4.2 Results

365

The results of the regional mappings were validated on downstream gauges following Huynh et al. (2024b). The spatio-temporal validation performance, which assesses the model outside of the calibration gauges and period, is particularly challenging at

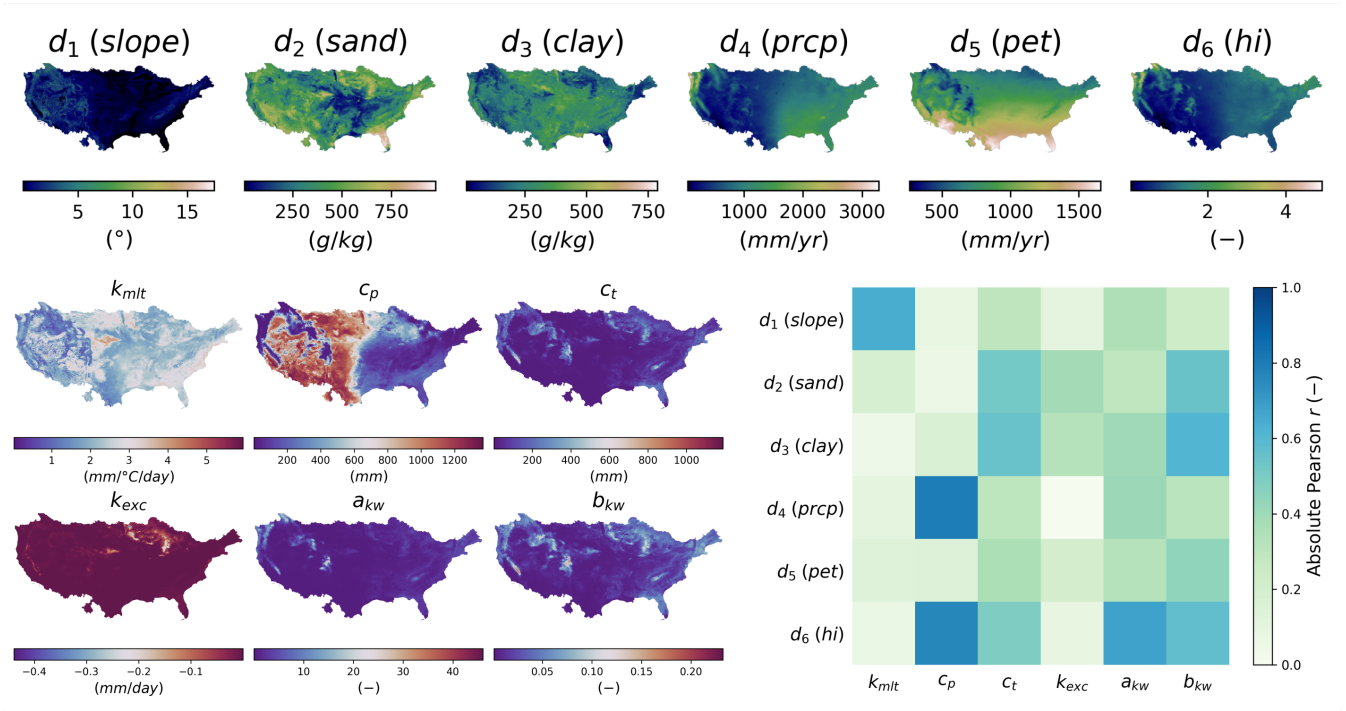


Figure 11. Analysis of input descriptors and output model parameters for the ANN mapping. Spatial distribution of physical descriptors (d_1 - d_6) on the top panel, details provided in (Tab. 3); spatial distribution of calibrated hydrological parameters (k_{mlt} , c_p , c_t , k_{exc} , a_{kw} , b_{kw}) on the lower left panel and linear correlation between descriptors and parameters on the lower right panel.

such a high resolution and given the complex variabilities of physical factors and hydrological responses over this Mediterranean flash flood-prone case. The results are shown in validation only, for brevity again, in Figure 13. A uniform mapping yields a poor median NSE of 0.15, while descriptors-to-parameters mappings achieve 0.62 and 0.69 for Multi-Linear and ANN approaches, respectively. Conceptual parameters maps obtained by learning from physical descriptors are shown in Figure 14 for the ANN mapping only (with the best NSE result). The correlation matrix highlights significant correlations, especially between production capacity (c_p) and topographic slope (d_5), as well as exchange parameter (k_{exc}) or routing parameter (a_{kw}) with topographic slope (d_5). For each parameter, a correlation is also found with vegetation cover rate (d_3) or forest cover rate (d_2). This illustrates the interpretability of our neural network-based regionalization algorithm, in the space of conceptual model parameters. A key feature of *smash* is its ability to accurately and efficiently compute spatially distributed cost gradients, as shown in Figure 16 in the conceptual parameter (θ) space for interpretability, in the case of a differentiable spatially distributed hydrological model including a NN-based regionalization mapping and a kinematic wave routing model (the partial differential equation numerical solver being also differentiated). Finally, simulated hydrographs are plotted for the six most downstream validation gauges in Figure 15 with a better reproduction for most downstream gauges in the present test

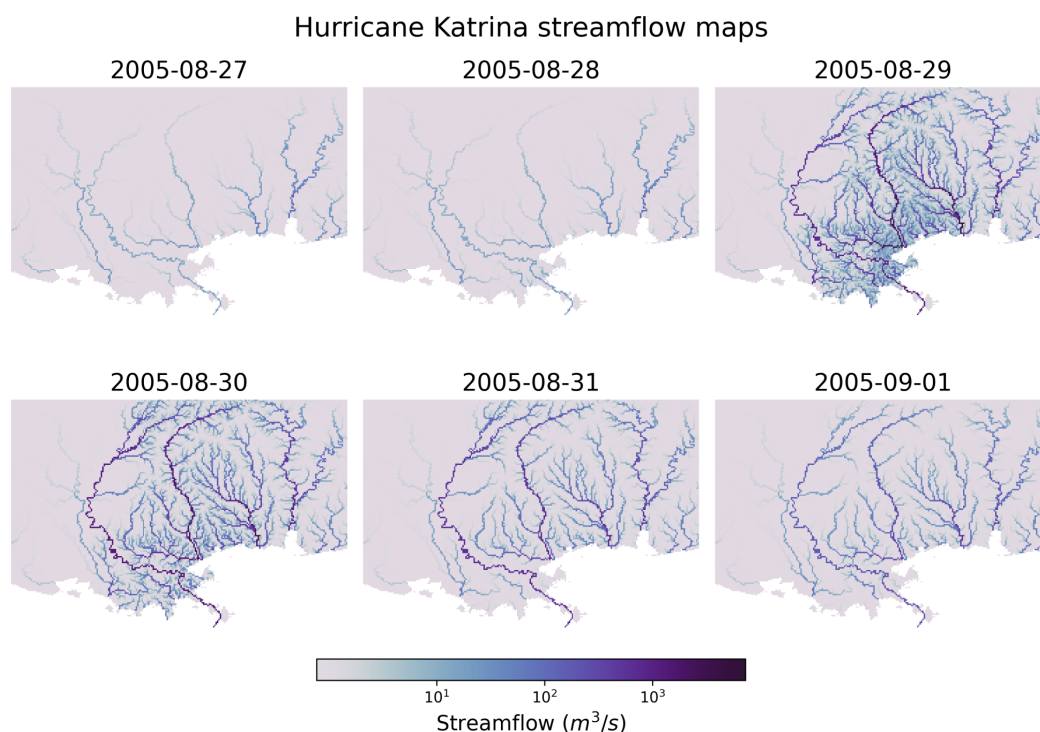


Figure 12. Streamflow dynamics during Hurricane Katrina from August 27 to September 1, 2005 for the ANN mapping. Each panel depicts the streamflow distribution across the affected region. To visualize the temporal evolution of the spatialized discharge pattern ; note that the kinematic wave routing was applied on flat topography, i.e. out of its validity range.

380 configuration with the calibrated ANN regionalization (coherent with results of Huynh et al. (2024b) over the whole French Mediterranean region).

These performances are very encouraging since they were obtained with a relatively simple regionalization setup on a complex flash flood-prone area. Further research with `smash` will focus on improving the versatility of the hydrological model, to better account for high rainfall intensities (e.g. Daniela Peredo and Oudin (2022)) or groundwater/karstic effects, with classical
 385 or hybrid differential equations capable to learn from data at multiple scales, and to enrich the regionalization algorithms with advanced cost functions and spatial relaxation/regularization strategies. These improvements are necessary to better extract information, with our variational data assimilation algorithm, from multiple discharge gauges and other data sources (descriptors, satellite moisture, temperature, etc.). Additionally, incorporating more realistic hydraulic routing embedded within the differentiable hydrologic model will also enable the integration of hydraulic information (water levels, flow videos, etc), as
 390 introduced in Pujol et al. (2022).

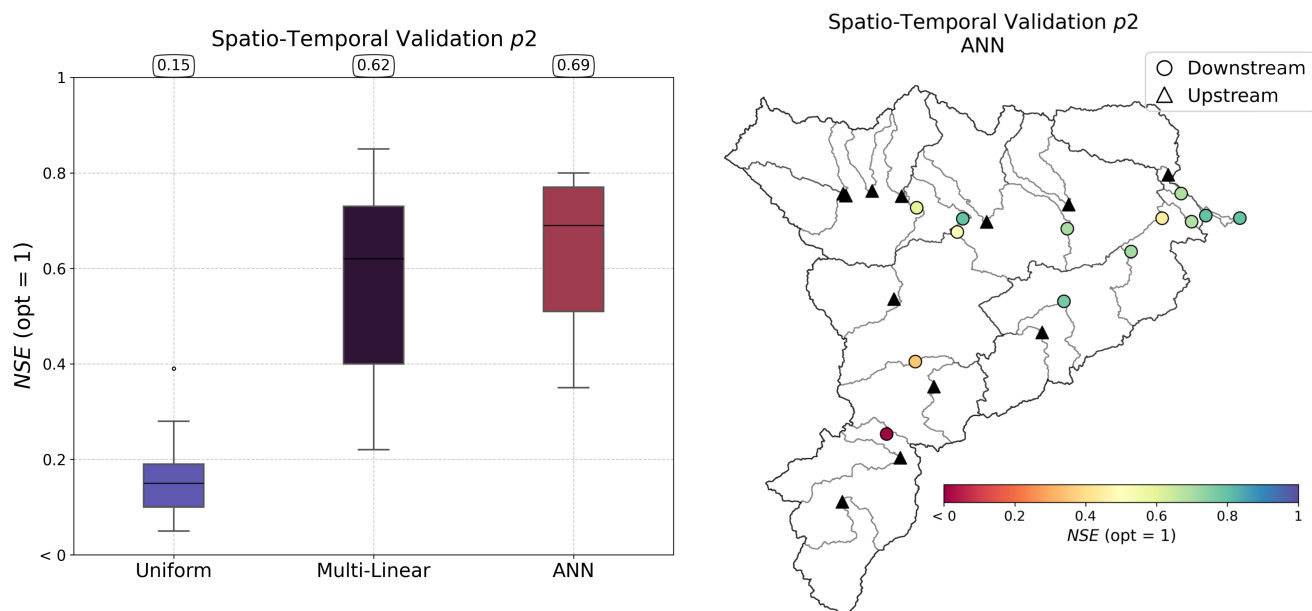


Figure 13. Performance in spatio-temporal validation over period p_2 using calibration on upstream gauges (triangles). The boxplots on the left panel represent the distribution of Nash-Sutcliffe Efficiency (NSE) scores for the three calibration methods: Uniform, Multi-Linear, and Artificial Neural Network (ANN). Median values are displayed at the top of each boxplot. The map on the right illustrates the spatial distribution of the NSE values for the ANN mapping for the downstream validation catchments.

5 Other smash features

In addition to the core differentiable spatialized hydrological solvers and regionalization learning algorithms illustrated above, smash enables performing:

- Automatic hydrograph segmentation and flood detection over large samples (Huynh et al., 2023).
- Parameter calibration using signature-based cost functions (Huynh et al., 2023) in addition to continuous metrics.
- Parameter calibration using a spatial regularization term (Jay-Allemand et al., 2020).
- Initial state estimation, including with regionalization mapping, even over short time windows which is applicable for short range .variational data assimilation for operational forecasting
- Simulation of discharge ensembles from rainfall ensemble forecasting.
- Bayesian approach for parameter estimation and uncertainty quantification, with the consideration of structural model error and observation errors.

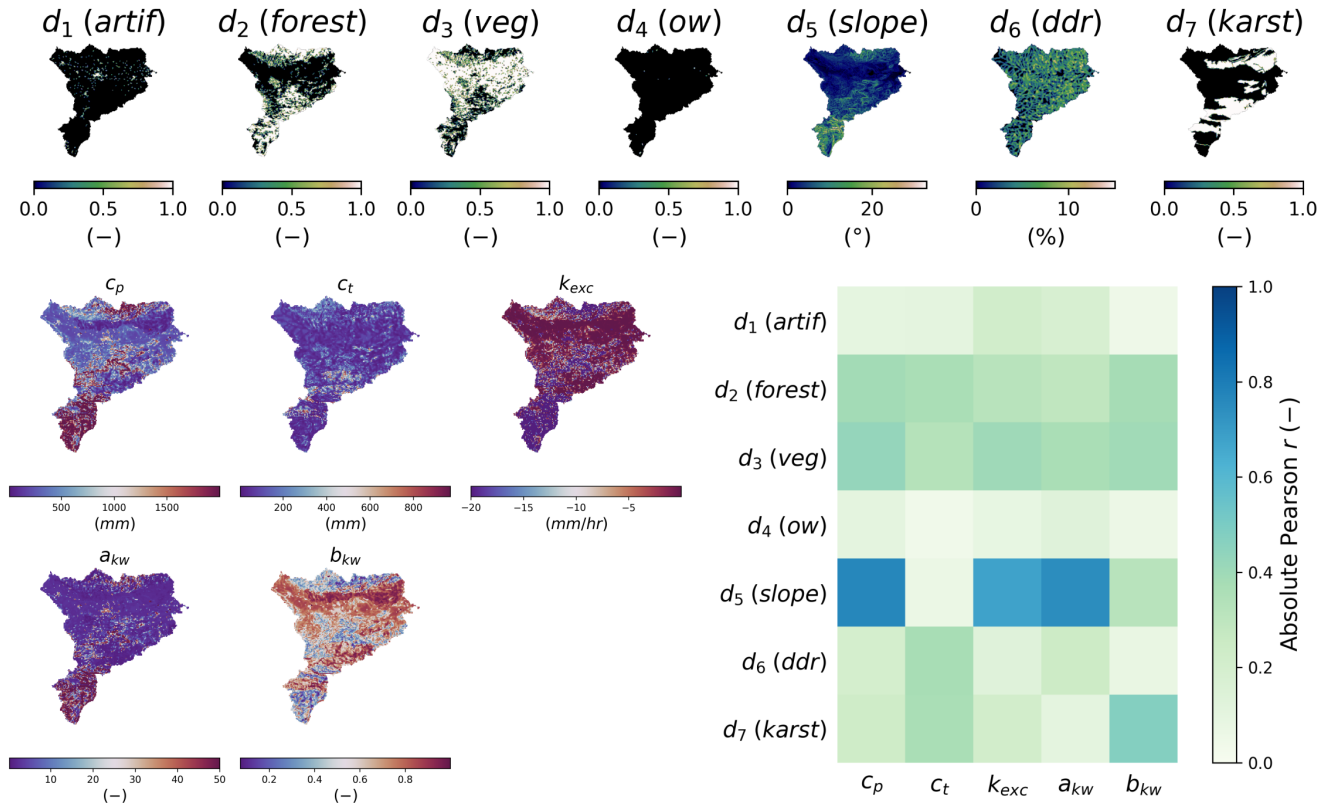


Figure 14. Analysis of input descriptors and output model parameters for the ANN descriptors-to-parameters mapping. Spatial distribution of physical descriptors (d_1 - d_7) on the top panel, details provided in (Tab. 4); Spatial distribution of calibrated hydrological parameters (c_p , c_t , k_{exc} , a_{kw} , b_{kw}) on the lower left panel and linear correlation between descriptors and parameters on the lower right panel.

6 Conclusions

The recently released `smash` framework represents a significant advancement in hydrological modeling and data assimilation. This conclusion synthesizes the key principles, implementation features, performance indicators, and future prospects of `smash`, as presented in this article.

`smash` is built around three foundational principles: a modular operator chaining, enabling flexible representation of vertical and lateral hydrological processes; a regionalization mapping through hybrid approaches, combining conceptual models with descriptors-to-parameters neural networks; and a robust inverse algorithm that support variational data assimilation.

The software leverages automatic differentiation to facilitate gradient-based calibration. Its seamless integration with Python via `f90wrap` ensures user-friendly access and flexibility, complemented by an automatic build system that simplifies deployment. Furthermore, `smash` supports parallel computing on CPUs, significantly accelerating computations for large-scale applications.

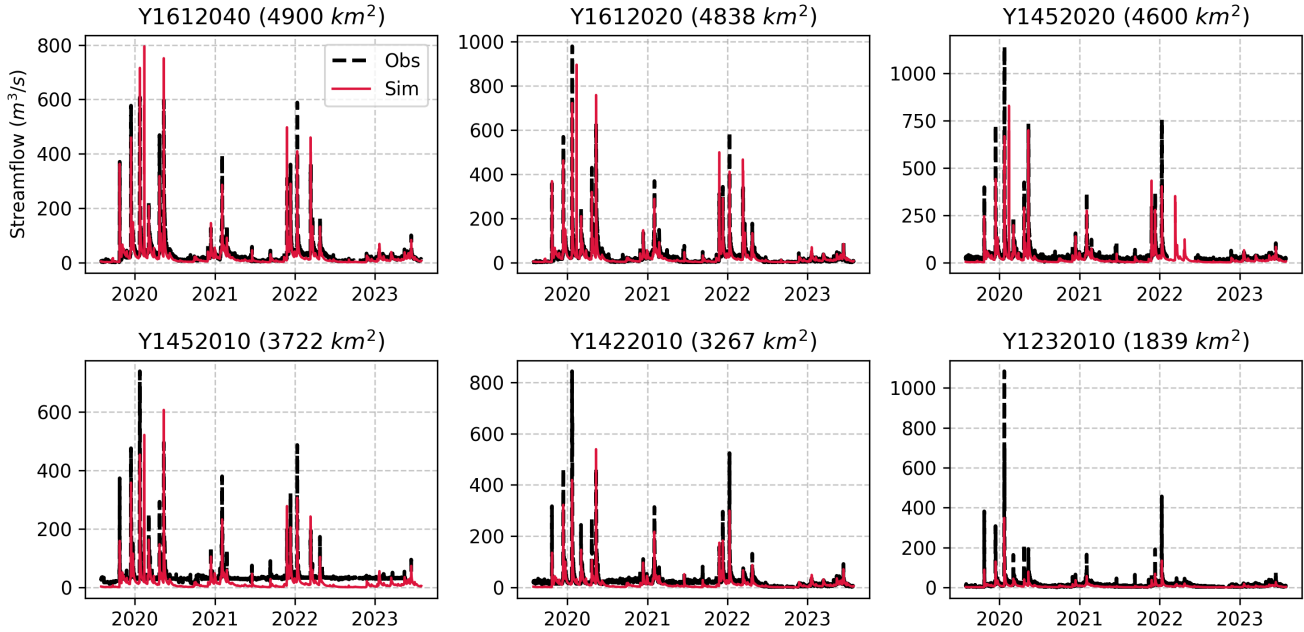


Figure 15. Observed and simulated streamflow of the six most downstream gauges of the Aude river for the ANN mapping. Each panel represents streamflow (m^3/s) for a specific gauge. Black dashed lines indicate observed values (Obs), while red solid lines represent simulated values (Sim).

In terms of hydrological modeling, *smash* achieves interesting results. Using CAMELS datasets, median $KGE > 0.8$ is observed in local spatially distributed calibration for daily GR-like and VIC-like model structures at $dx = 1'30''$ ($\sim 3km$). Additionally, regionalization learning across CONUS of conceptual parameters from physical descriptors yields $KGE > 0.6$ in spatio-temporal validation. High-resolution hourly modeling at $dx = 500m$ for Mediterranean flash-flood scenarios demonstrates $NSE > 0.6$.

smash planned enhancements include the integration of additional differentiable hydrological and hydraulic models, the expansion of hybrid physics-AI frameworks, and the refinement of data assimilation techniques. These advancements aim to further improve model accuracy, computational efficiency, and applicability in both research and operational settings.

Code and data availability. The source code of *smash*, Version 1.0, is available and preserved on multiple platforms: GitHub at <https://github.com/DassHydro/smash/tree/v1.0.2>, PyPI at <https://pypi.org/project/hydro-smash/1.0.2>, and Zenodo with the DOI <https://doi.org/10.5281/zenodo.14841726> (Colleoni et al., 2025a). The datasets presented in this paper are also available on Zenodo under the DOI <https://doi.org/10.5281/zenodo.14865491> (Colleoni et al., 2025b). *smash* is released under the GPL-3 license and is developed openly at <https://github.com/DassHydro/smash>. The documentation is accessible at <https://smash.recover.inrae.fr>.

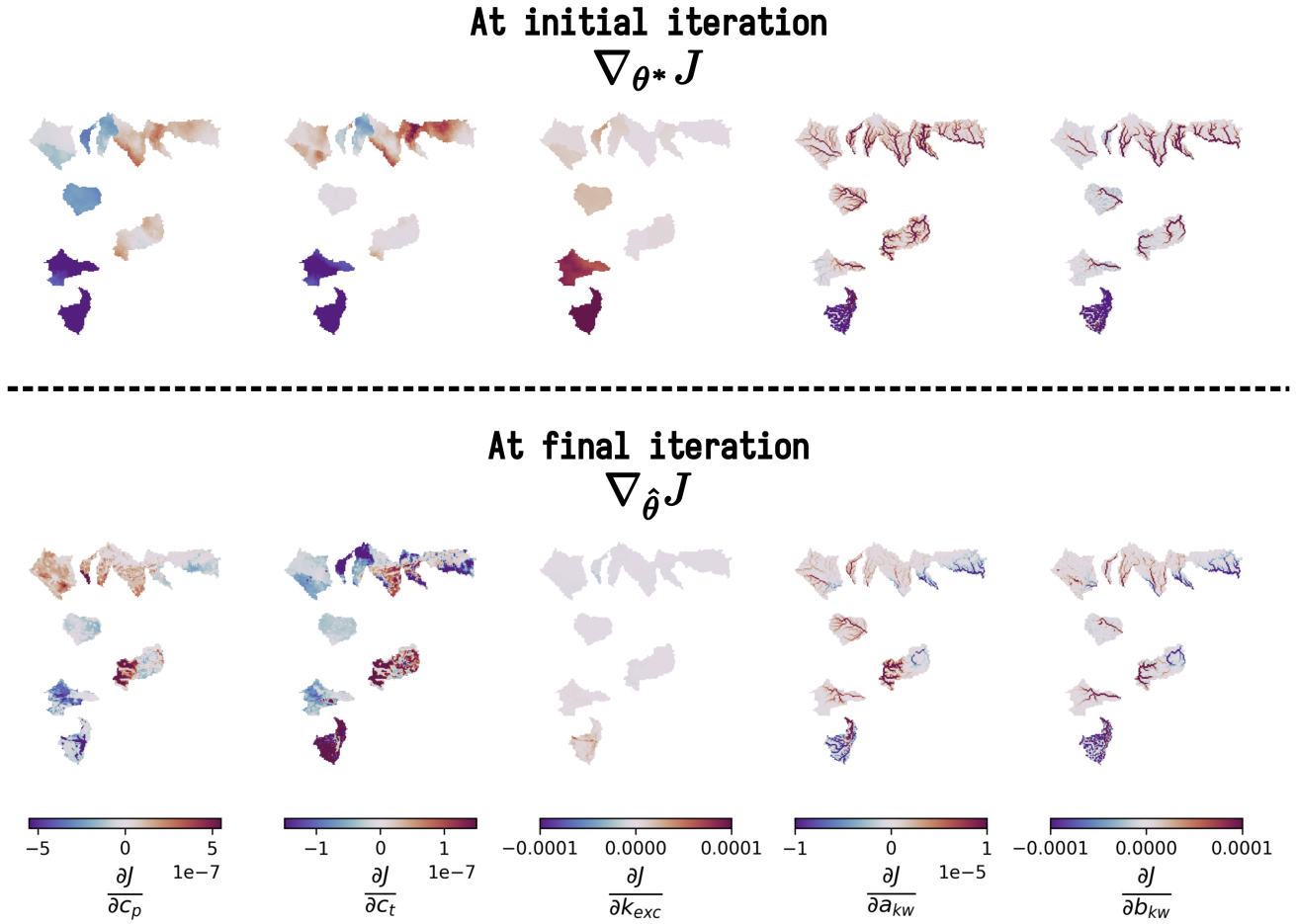


Figure 16. Spatially distributed gradients of the cost function J with respect to the model parameters at initial and final iterations for ANN mapping. The first row shows the gradients $\nabla_{\theta^*} J$ at the initial iteration, while the second row presents the gradients $\nabla_{\hat{\theta}} J$ at the final iteration after optimization. Each column corresponds to the partial derivative of J with respect to a specific parameter: c_p , c_t , k_{exc} , a_{kw} , and b_{kw} . These gradients are used in the optimization process of the control vector ρ using $\nabla_{\rho} J = \nabla_{\theta} J \cdot \nabla_{\rho} \theta$ with $\theta = \mathcal{N}(\cdot, \rho)$ where \mathcal{N} is the multi-layer perceptron used.



Table A1. Median KGE obtained in regionalization mapping calibration-validation over 4 groups of randomly selected basins.

Group	Calibration KGE_{50}	Spatial Validation KGE_{50}	Temporal Validation KGE_{50}	Spatio-Temporal Validation KGE_{50}
0	0.65	0.62	0.65	0.65
1	0.62	0.58	0.65	0.58
2	0.65	0.65	0.64	0.67
3	0.65	0.63	0.65	0.63

Appendix A

A1 CONUS - CAMELS - Regionalization

Appendix B

B1 CPU Information

```

430 Architecture:          x86_64
    CPU op-mode(s):      32-bit, 64-bit
    Address sizes:       48 bits physical, 48 bits virtual
    Byte Order:          Little Endian
    CPU(s):              192
435   On-line CPU(s) list: 0-191
    Vendor ID:           AuthenticAMD
    Model name:          AMD EPYC 7643 48-Core Processor
    CPU family:          25
    Model:               1
440   Thread(s) per core: 2
    Core(s) per socket:  48
    Socket(s):           2
    Stepping:            1
    Frequency boost:     enabled
445   CPU max MHz:        2300.0000
    CPU min MHz:         1500.0000
    BogoMIPS:            4591.48
    Virtualization features:
    Virtualization:      AMD-V

```




450 Caches (sum of all):

L1d:	3 MiB (96 instances)
L1i:	3 MiB (96 instances)
L2:	48 MiB (96 instances)
L3:	512 MiB (16 instances)

455 NUMA:

NUMA node(s) :	2
NUMA node0 CPU(s) :	0-47, 96-143
NUMA node1 CPU(s) :	48-95, 144-191

460 *Author contributions.* FC: lead developer of *smash* v1.0, conceptualization, numerical experiments and results analysis, manuscript preparation. NNTH: main developer of *smash* v1.0, conceptualization, results analysis, manuscript preparation. PAG: co-developer, conceptualization, research plan and supervision, results analysis, manuscript preparation, funding. MJA: co-developer of *smash* v1.0, main developer of the first wrapping and differentiable code, manuscript review. DO: main developer of the first Fortran code, manuscript review. BR: co-developer of *smash* v1.0, results analysis, research co-supervision, manuscript review. TDF, AEB, JD: contribution to co-developement of *smash* v1.0, manuscript review. PJ: results analysis, manuscript review, funding.

465 *Competing interests.* The authors declare no competing interests

Acknowledgements. The French national flood forecasting center, Service Central Vigicrues (ex. SCHAPI), is greatly acknowledged for funding research, software development and operational application, for long term collaboration on flood forecasting and data sharing. This work was also supported by funding from ANR grant ANR-21-CE04-0021-01 (MUFFINS project, "MULTIscale Flood Forecasting with INnovating Solutions"). During the preparation of this work, the authors used Mistral AI in order to correct and improve English language.

470 After using this tool, the authors reviewed and edited the content as needed and takes full responsibility for the content of the publication.



References

- Addor, N., Newman, A. J., Mizukami, N., and Clark, M. P.: The CAMELS data set: catchment attributes and meteorology for large-sample studies, *Hydrology and Earth System Sciences*, 21, 5293–5313, <https://doi.org/10.5194/hess-21-5293-2017>, 2017.
- Aerts, J. P. M., Hut, R. W., van de Giesen, N. C., Drost, N., van Verseveld, W. J., Weerts, A. H., and Hazenberg, P.: Large-sample assessment
475 of varying spatial resolution on the streamflow estimates of the wflow_sbm hydrological model, *Hydrology and Earth System Sciences*, 26, 4407–4430, <https://doi.org/10.5194/hess-26-4407-2022>, 2022.
- Andréassian, V., Perrin, C., Berthet, L., Le Moine, N., Lerat, J., Loumagne, C., Oudin, L., Mathevet, T., Ramos, M.-H., and Valéry, A.: HESS Opinions "Crash tests for a standardized evaluation of hydrological models", *Hydrology and Earth System Sciences*, 13, 1757–1764, <https://doi.org/10.5194/hess-13-1757-2009>, 2009.
- 480 Beck, H. E., van Dijk, A. I. J. M., de Roo, A., Miralles, D. G., McVicar, T. R., Schellekens, J., and Bruijnzeel, L. A.: Global-scale regionalization of hydrologic model parameters, *Water Resources Research*, 52, 3599–3622, <https://doi.org/10.1002/2015WR018247>, 2016.
- Beck, H. E., Wood, E. F., Pan, M., Fisher, C. K., Miralles, D. G., van Dijk, A. I. J. M., McVicar, T. R., and Adler, R. F.: MSWEP V2 Global 3-Hourly 0.1° Precipitation: Methodology and Quantitative Assessment, *Bulletin of the American Meteorological Society*, 100, 473 – 500, <https://doi.org/10.1175/BAMS-D-17-0138.1>, 2019.
- 485 Beck, H. E., Pan, M., Lin, P., Seibert, J., van Dijk, A. I. J. M., and Wood, E. F.: Global Fully Distributed Parameter Regionalization Based on Observed Streamflow From 4,229 Headwater Catchments, *Journal of Geophysical Research: Atmospheres*, 125, e2019JD031485, <https://doi.org/10.1029/2019JD031485>, e2019JD031485 10.1029/2019JD031485, 2020.
- Bertalanffy, L. v.: General system theory: Foundations, development, applications, G. Braziller, 1968.
- Beven, K.: Towards a new paradigm in hydrology, IN: *Water for the Future: Hydrology in Perspective*. IAHS Publication, 1987.
- 490 Beven, K.: Changing ideas in hydrology — The case of physically-based models, *Journal of Hydrology*, 105, 157–172, [https://doi.org/10.1016/0022-1694\(89\)90101-7](https://doi.org/10.1016/0022-1694(89)90101-7), 1989.
- Beven, K.: Prophecy, reality and uncertainty in distributed hydrological modelling., *Advances in Water Resources*, 16, 41–51, [https://doi.org/10.1016/0309-1708\(93\)90028-E](https://doi.org/10.1016/0309-1708(93)90028-E), 1993.
- Beven, K.: How far can we go in distributed hydrological modelling?, *Hydrology and Earth System Sciences*, 5, 1–12, <https://doi.org/10.5194/hess-5-1-2001>, 2001.
- 495 Beven, K. J.: *Rainfall - Runoff Modelling, The Primer*, John Wiley and Sons, LTD, 2011.
- Bierkens, M. F. P., Bell, V. A., Burek, P., Chaney, N., Condon, L. E., David, C. H., de Roo, A., Döll, P., Drost, N., Famiglietti, J. S., Flörke, M., Gochis, D. J., Houser, P., Hut, R., Keune, J., Kollet, S., Maxwell, R. M., Reager, J. T., Samaniego, L., Sudicky, E., Sutanudjaja, E. H., van de Giesen, N., Winsemius, H., and Wood, E. F.: Hyper-resolution global hydrological modelling: what is next?, *Hydrological Processes*, 29, 310–320, <https://doi.org/10.1002/hyp.10391>, 2015.
- 500 Blöschl, G. and Sivapalan, M.: Scale issues in hydrological modelling: A review, *Hydrological Processes*, 9, 251–290, <https://doi.org/10.1002/hyp.3360090305>, 1995.
- Bouaziz, L. J. E., Fenicia, F., Thirel, G., de Boer-Euser, T., Buitink, J., Brauer, C. C., De Niel, J., Dewals, B. J., Drogue, G., Grelier, B., Melsen, L. A., Moustakas, S., Nossent, J., Pereira, F., Sprockereef, E., Stam, J., Weerts, A. H., Willems, P., Savenije, H. H. G., and Hrachowitz, M.: Behind the scenes of streamflow model performance, *Hydrology and Earth System Sciences*, 25, 1069–1095, <https://doi.org/10.5194/hess-25-1069-2021>, 2021.
- 505



- Brisset, P., Monnier, J., Garambois, P.-A., and Roux, H.: On the assimilation of altimetric data in 1D Saint-Venant river flow models, *Advances in water resources*, 119, 41–59, <https://doi.org/10.1016/j.advwatres.2018.06.004>, 2018.
- Castaings, W., Dartus, D., Le Dimet, F.-X., and Saulnier, G.-M.: Sensitivity analysis and parameter estimation for distributed hydrological modeling: potential of variational methods, *Hydrology and Earth System Sciences*, 13, 503 – 517, 2009.
- Champeaux, J.-L., Dupuy, P., Laurantin, O., Soulan, I., Tabary, P., and Soubeyroux, J.-M.: Les mesures de précipitations et l'estimation des lames d'eau à Météo-France : état de l'art et perspectives, *La Houille Blanche*, 95, 28–34, <https://doi.org/10.1051/lhb/2009052>, 2009.
- Chow, V. T., Maidment, D. R., and Mays, L. W.: *Applied Hydrology*, McGraw-Hill Series in Water Resources and Environmental Engineering, 1998.
- Clark, M. P., Bierkens, M. F., Samaniego, L., Woods, R. A., Uijlenhoet, R., Bennett, K. E., Pauwels, V., Cai, X., Wood, A. W., and Peters-Lidard, C. D.: The evolution of process-based hydrologic models: historical challenges and the collective quest for physical realism, *Hydrology and Earth System Sciences*, 21, 3427–3440, 2017.
- Colleoni, F., Garambois, P.-A., Javelle, P., Jay-Allemand, M., and Arnaud, P.: Adjoint-based spatially distributed calibration of a grid GR-based parsimonious hydrological model over 312 French catchments with SMASH platform, *EGUsphere*, 2022, 1–37, <https://doi.org/10.5194/egusphere-2022-506>, 2022.
- Colleoni, F., Huynh, N. N. T., Garambois, P.-A., Jay-Allemand, M., Organde, D., Renard, B., De Fournas, T., El Baz, A., Demargne, J., and Javelle, P.: SMASH v1.0.2, <https://doi.org/10.5281/zenodo.14841726>, 2025a.
- Colleoni, F., Huynh, N. N. T., Garambois, P.-A., Jay-Allemand, M., Organde, D., Renard, B., De Fournas, T., El Baz, A., Demargne, J., and Javelle, P.: SMASH v1.0.2 cases, <https://doi.org/10.5281/zenodo.14865491>, 2025b.
- Dagum, L. and Menon, R.: OpenMP: an industry standard API for shared-memory programming, *IEEE Computational Science and Engineering*, 5, 46–55, <https://doi.org/10.1109/99.660313>, 1998.
- Daniela Peredo, Maria-Helena Ramos, V. A. and Oudin, L.: Investigating hydrological model versatility to simulate extreme flood events, *Hydrological Sciences Journal*, 67, 628–645, <https://doi.org/10.1080/02626667.2022.2030864>, 2022.
- De Lavenne, A., Andréassian, V., Thirel, G., Ramos, M.-H., and Perrin, C.: A regularization approach to improve the sequential calibration of a semidistributed hydrological model, *Water Resources Research*, 55, 8821–8839, 2019.
- Dooge, J. C. I.: Looking for hydrologic laws, *Water Resources Research*, 22, 46S–58S, <https://doi.org/10.1029/WR022i09Sp0046S>, 1986.
- Duan, Q., Schaake, J., Andréassian, V., Franks, S., Goteti, G., Gupta, H., Gusev, Y., Habets, F., Hall, A., Hay, L., Hogue, T., Huang, M., Leavesley, G., Liang, X., Nasonova, O., Noilhan, J., Oudin, L., Sorooshian, S., Wagener, T., and Wood, E.: Model Parameter Estimation Experiment (MOPEX): An overview of science strategy and major results from the second and third workshops, *Journal of Hydrology*, 320, 3–17, <https://doi.org/10.1016/j.jhydrol.2005.07.031>, the model parameter estimation experiment, 2006.
- Eilander, D.: pyFlwDir, <https://doi.org/10.5281/zenodo.7759261>, 2023.
- Eilander, D., van Verseveld, W., Yamazaki, D., Weerts, A., Winsemius, H. C., and Ward, P. J.: A hydrography upscaling method for scale-invariant parametrization of distributed hydrological models, *Hydrology and Earth System Sciences*, 25, 5287–5313, <https://doi.org/10.5194/hess-25-5287-2021>, 2021.
- Feng, D., Beck, H., de Bruijn, J., Sahu, R. K., Satoh, Y., Wada, Y., Liu, J., Pan, M., Lawson, K., and Shen, C.: Deep dive into hydrologic simulations at global scale: harnessing the power of deep learning and physics-informed differentiable models (δ HBV-globe1.0-hydroDL), *Geoscientific Model Development*, 17, 7181–7198, <https://doi.org/10.5194/gmd-17-7181-2024>, 2024.
- Fenicia, F., Kavetski, D., and Savenije, H. H.: Elements of a flexible approach for conceptual hydrological modeling: 1. Motivation and theoretical development, *Water Resources Research*, 47, 2011.



- 545 Ficchi, A., Perrin, C., and Andréassian, V.: Hydrological modelling at multiple sub-daily time steps: Model improvement via flux-matching, *Journal of Hydrology*, 575, 1308–1327, <https://doi.org/10.1016/j.jhydrol.2019.05.084>, 2019.
- Folton, N. and Arnaud, P.: Indicateurs sur la ressource en eau estimés par une modélisation pluie-débit régionalisée: la base de données Web LoiEau, *La Houille Blanche*, 106, 22–29, <https://doi.org/10.1051/lhb/2020034>, 2020.
- Garavaglia, F., Le Lay, M., Gottardi, F., Garçon, R., Gailhard, J., Paquet, E., and Mathevet, T.: Impact of model structure on flow simulation and hydrological realism: from a lumped to a semi-distributed approach, *Hydrology and Earth System Sciences*, 21, 3937–3952, <https://doi.org/10.5194/hess-21-3937-2017>, 2017.
- 550 Gupta, H. V., Kling, H., Yilmaz, K. K., and Martinez, G. F.: Decomposition of the mean squared error and NSE performance criteria: Implications for improving hydrological modelling, *Journal of Hydrology*, 377, 80–91, <https://doi.org/10.1016/j.jhydrol.2009.08.003>, 2009.
- Gupta, H. V., Perrin, C., Blöschl, G., Montanari, A., Kumar, R., Clark, M., and Andréassian, V.: Large-sample hydrology: a need to balance depth with breadth, *Hydrology and Earth System Sciences*, 18, 463–477, <https://doi.org/10.5194/hess-18-463-2014>, 2014.
- 555 Harris, C. R., Millman, K. J., van der Walt, S. J., Gommers, R., Virtanen, P., Cournapeau, D., Wieser, E., Taylor, J., Berg, S., Smith, N. J., Kern, R., Picus, M., Hoyer, S., van Kerkwijk, M. H., Brett, M., Haldane, A., del Río, J. F., Wiebe, M., Peterson, P., Gérard-Marchant, P., Sheppard, K., Reddy, T., Weckesser, W., Abbasi, H., Gohlke, C., and Oliphant, T. E.: Array programming with NumPy, *Nature*, 585, 357–362, <https://doi.org/10.1038/s41586-020-2649-2>, 2020.
- 560 Hascoet, L. and Pascual, V.: The Tapenade automatic differentiation tool: principles, model, and specification, *ACM Transactions on Mathematical Software (TOMS)*, 39, 1–43, 2013.
- Hengl, T., Mendes de Jesus, J., Heuvelink, G. B. M., Ruiperez Gonzalez, M., Kilibarda, M., Blagotić, A., Shangguan, W., Wright, M. N., Geng, X., Bauer-Marschallinger, B., Guevara, M. A., Vargas, R., MacMillan, R. A., Batjes, N. H., Leenaars, J. G. B., Ribeiro, E., Wheeler, I., Mantel, S., and Kempen, B.: SoilGrids250m: Global gridded soil information based on machine learning, *PLOS ONE*, 12, 1–40, <https://doi.org/10.1371/journal.pone.0169748>, 2017.
- 565 Hersbach, H., Bell, B., Berrisford, P., Hirahara, S., Horányi, A., Muñoz-Sabater, J., Nicolas, J., Peubey, C., Radu, R., Schepers, D., Simmons, A., Soci, C., Abdalla, S., Abellan, X., Balsamo, G., Bechtold, P., Biavati, G., Bidlot, J., Bonavita, M., De Chiara, G., Dahlgren, P., Dee, D., Diamantakis, M., Dragani, R., Flemming, J., Forbes, R., Fuentes, M., Geer, A., Haimberger, L., Healy, S., Hogan, R. J., Hólm, E., Janisková, M., Keeley, S., Laloyaux, P., Lopez, P., Lupu, C., Radnoti, G., de Rosnay, P., Rozum, I., Vamborg, F., Villaume, S., and Thépaut, J.-N.: The ERA5 global reanalysis, *Quarterly Journal of the Royal Meteorological Society*, 146, 1999–2049, <https://doi.org/10.1002/qj.3803>, 2020.
- Hrachowitz, M. and Clark, M. P.: HESS Opinions: The complementary merits of competing modelling philosophies in hydrology, *Hydrology and Earth System Sciences*, 21, 3953–3973, 2017.
- 575 Huynh, N. N. T., Garambois, P.-A., Colleoni, F., and Javelle, P.: Signatures-and-sensitivity-based multi-criteria variational calibration for distributed hydrological modeling applied to Mediterranean floods, *Journal of Hydrology*, 625, 129992, <https://doi.org/10.1016/j.jhydrol.2023.129992>, 2023.
- Huynh, N. N. T., Garambois, P.-A., Colleoni, F., Renard, B., Monnier, J., and Roux, H.: Multiscale Learnable Physical Modeling and Data Assimilation Framework: Application to High-Resolution Regionalized Hydrological Simulation of Flash Flood, *Authorea Preprints*, <https://doi.org/10.22541/au.170709054.44271526/v2>, 2024a.
- 580 Huynh, N. N. T., Garambois, P.-A., Colleoni, F., Renard, B., Roux, H., Demargne, J., Jay-Allemand, M., and Javelle, P.: Learning Regionalization Using Accurate Spatial Cost Gradients Within a Differentiable High-Resolution Hydrological Model: Application to the French



- Mediterranean Region, *Water Resources Research*, 60, e2024WR037544, <https://doi.org/10.1029/2024WR037544>, e2024WR037544 2024WR037544, 2024b.
- Huynh, N. N. T., Garambois, P.-A., Renard, B., Colleoni, F., Monnier, J., and Roux, H.: A Distributed Hybrid Physics-AI Framework for Learning Corrections of Internal Hydrological Fluxes and Enhancing High-Resolution Regionalized Flood Modeling, <https://doi.org/10.5194/egusphere-2024-3665>, 2025.
- Jay-Allemand, M., Javelle, P., Gejadze, I., Arnaud, P., Malaterre, P.-O., Fine, J.-A., and Organde, D.: On the potential of variational calibration for a fully distributed hydrological model: application on a Mediterranean catchment, *Hydrology and Earth System Sciences*, 24, 5519–5538, 2020.
- Jay-Allemand, M., Colleoni, F., Garambois, P.-A., Javelle, P., and Demargne, J.: SMASH - Spatially distributed Modelling and ASsimilation for Hydrology: Python wrapping towards enhances research-to-operations transfer, *IAHS 2022 - Montpellier*, <https://hal.science/hal-03683657>, poster, 2022.
- Jay-Allemand, M., Demargne, J., Garambois, P.-A., Javelle, P., Gejadze, I., Colleoni, F., Organde, D., Arnaud, P., and Fouchier, C.: Spatially distributed calibration of a hydrological model with variational optimization constrained by physiographic maps for flash flood forecasting in France, *Proceedings of IAHS*, 385, 281–290, <https://doi.org/10.5194/piahs-385-281-2024>, 2024.
- Kermode, J. R.: f90wrap: an automated tool for constructing deep Python interfaces to modern Fortran codes, *J. Phys. Condens. Matter*, <https://doi.org/10.1088/1361-648X/ab82d2>, 2020.
- Kingma, D. P. and Ba, J.: Adam: A method for stochastic optimization, *arXiv preprint arXiv:1412.6980*, 2014.
- Klemeš, V.: Conceptualization and scale in hydrology, *Journal of Hydrology*, 65, 1–23, [https://doi.org/10.1016/0022-1694\(83\)90208-1](https://doi.org/10.1016/0022-1694(83)90208-1), scale Problems in Hydrology, 1983.
- Kratzert, F., Nearing, G., Addor, N., Erickson, T., Gauch, M., Gilon, O., Gudmundsson, L., Hassidim, A., Klotz, D., Nevo, S., Shalev, G., and Matias, Y.: Caravan - A global community dataset for large-sample hydrology, *Scientific Data*, 10, 61, <https://doi.org/10.1038/s41597-023-01975-w>, 2023.
- Lane, R. A., Coxon, G., Freer, J. E., Wagener, T., Johnes, P. J., Bloomfield, J. P., Greene, S., Macleod, C. J. A., and Reaney, S. M.: Benchmarking the predictive capability of hydrological models for river flow and flood peak predictions across over 1000 catchments in Great Britain, *Hydrology and Earth System Sciences*, 23, 4011–4032, <https://doi.org/10.5194/hess-23-4011-2019>, 2019.
- Le Moine, N.: Le bassin versant de surface vu par le souterrain : une voie d’amélioration des performances et du réalisme des modèles pluie-débit ?, Ph.D. thesis, Cemagref (UR HBAN, Antony), 2008.
- Leblois, E. and Sauquet, E.: Grid elevation models in hydrology - Part 1: Principales and literature review; Part 2: HydroDEM, User’s manual, Tech. rep., Cemagref, 1999.
- Liang, X., Lettenmaier, D. P., Wood, E. F., and Burges, S. J.: A simple hydrologically based model of land surface water and energy fluxes for general circulation models, *Journal of Geophysical Research: Atmospheres*, 99, 14 415–14 428, <https://doi.org/10.1029/94JD00483>, 1994.
- Liu, Y. and Gupta, H. V.: Uncertainty in hydrologic modeling: Toward an integrated data assimilation framework, *Water resources research*, 43, 2007.
- Mathevet, T.: Quels modèles pluie-débit globaux au pas de temps horaire? Développements empiriques et intercomparaison de modèles sur un large échantillon de bassins versants, Ph.D. thesis, Ph. D. thesis, ENGREF, 463 pp, 2005.



- Mathevet, T., Gupta, H., Perrin, C., Andréassian, V., and Le Moine, N.: Assessing the performance and robustness of two conceptual rainfall-runoff models on a worldwide sample of watersheds, *Journal of Hydrology*, 585, 124 698, <https://doi.org/10.1016/j.jhydrol.2020.124698>, 2020.
- Milly, P.: Climate, interseasonal storage of soil water, and the annual water balance, *Advances in Water Resources*, 17, 19–24, [https://doi.org/10.1016/0309-1708\(94\)90020-5](https://doi.org/10.1016/0309-1708(94)90020-5), MIT Colloquium on Hydroclimatology and Global Hydrology, 1994.
- Mizukami, N., Clark, M. P., Newman, A. J., Wood, A. W., Gutmann, E. D., Nijssen, B., Rakovec, O., and Samaniego, L.: Towards seamless large-domain parameter estimation for hydrologic models, *Water Resources Research*, 53, 8020–8040, <https://doi.org/10.1002/2017WR020401>, 2017.
- Mizukami, N., Rakovec, O., Newman, A. J., Clark, M. P., Wood, A. W., Gupta, H. V., and Kumar, R.: On the choice of calibration metrics for “high-flow” estimation using hydrologic models, *Hydrology and Earth System Sciences*, 23, 2601–2614, <https://doi.org/10.5194/hess-23-2601-2019>, 2019.
- Monnier, J.: Data Assimilation - Inverse Problems, Assimilation, Control, Learning, INSA Toulouse, <https://www.math.univ-toulouse.fr/~jmonnie/Enseignement/CourseVDA.pdf>, 2024.
- Monnier, J., Couderc, F., Dartus, D., Larnier, K., Madec, R., and Vila, J.-P.: Inverse algorithms for 2D shallow water equations in presence of wet dry fronts: Application to flood plain dynamics, *Advances in Water Resources*, 97, 11–24, <https://doi.org/10.1016/j.advwatres.2016.07.005>, 2016.
- Newman, A. J., Clark, M. P., Sampson, K., Wood, A., Hay, L. E., Bock, A., Viger, R. J., Blodgett, D., Brekke, L., Arnold, J. R., Hopson, T., and Duan, Q.: Development of a large-sample watershed-scale hydrometeorological data set for the contiguous USA: data set characteristics and assessment of regional variability in hydrologic model performance, *Hydrology and Earth System Sciences*, 19, 209–223, <https://doi.org/10.5194/hess-19-209-2015>, 2015.
- Organde, D., Arnaud, P., Fine, J.-A., Fouchier, C., Folton, N., and Lavabre, J.: Régionalisation d’une méthode de prédétermination de crue sur l’ensemble du territoire français: la méthode SHYREG, *Revue des Sciences de l’Eau*, 26, 65–78, 2013.
- Orth, R., Staudinger, M., Seneviratne, S. I., Seibert, J., and Zappa, M.: Does model performance improve with complexity? A case study with three hydrological models, *Journal of Hydrology*, 523, 147–159, <https://doi.org/10.1016/j.jhydrol.2015.01.044>, 2015.
- Oudin, L., Hervieu, F., Michel, C., Perrin, C., Andréassian, V., Anctil, F., and Loumagne, C.: Which potential evapotranspiration input for a lumped rainfall–runoff model?: Part 2—Towards a simple and efficient potential evapotranspiration model for rainfall–runoff modelling, *Journal of Hydrology*, 303, 290–306, <https://doi.org/10.1016/j.jhydrol.2004.08.026>, 2005.
- pandas development team, T.: pandas-dev/pandas: Pandas, <https://doi.org/10.5281/zenodo.3509134>, 2020.
- Perrin, C., Michel, C., and Andréassian, V.: Does a large number of parameters enhance model performance? Comparative assessment of common catchment model structures on 429 catchments, *Journal of Hydrology*, 242, 275–301, [https://doi.org/10.1016/S0022-1694\(00\)00393-0](https://doi.org/10.1016/S0022-1694(00)00393-0), 2001.
- Perrin, C., Michel, C., and Andréassian, V.: Improvement of a parsimonious model for streamflow simulation, *Journal of hydrology*, 279, 275–289, 2003.
- Piotte, O., Montmerle, T., Fouchier, C., Belleudy, A., Garandeau, L., Janet, B., Jauffret, C., Demargne, J., and Organde, D.: Les évolutions du service d’avertissement sur les pluies intenses et les crues soudaines en France☆, *La Houille Blanche*, 106, 75–84, <https://doi.org/10.1051/lhb/2020055>, 2020.
- Pujol, L., Garambois, P.-A., and Monnier, J.: Multi-dimensional hydrological-hydraulic model with variational data assimilation for river networks and floodplains, *EGUsphere*, 2022, 1–44, <https://doi.org/10.5194/egusphere-2022-10>, 2022.



- Quintana-Seguí, P., Le Moigne, P., Durand, Y., Martin, E., Habets, F., Baillon, M., Canellas, C., Franchisteguy, L., and Morel, S.: Analysis of Near-Surface Atmospheric Variables: Validation of the SAFRAN Analysis over France, *Journal of Applied Meteorology and Climatology*, 47, 92, <https://doi.org/10.1175/2007JAMC1636.1>, 2008.
- Reed, S., Koren, V., Smith, Z., Moreda, Fekadu, Seo, Dong-Jun, Butts, M., and DMIP: Reed S., Koren V., Smith M. Zhang Z, Moreda F, Seo D-J and DMIP Participants (Butts M. B), 2004: Overall distributed model intercomparison project results, *Journal of Hydrology*, Volume 298, Issues 1-4, 1 October 2004, Pages 27-60., *Journal of Hydrology*, 298, 27–60, 2004.
- Refsgaard, J. C.: Parameterisation, calibration and validation of distributed hydrological models, *Journal of Hydrology*, 198, 69–97, [https://doi.org/10.1016/S0022-1694\(96\)03329-X](https://doi.org/10.1016/S0022-1694(96)03329-X), 1997.
- Samaniego, L., Kumar, R., and Attinger, S.: Multiscale parameter regionalization of a grid-based hydrologic model at the mesoscale, *Water Resources Research*, 46, <https://doi.org/10.1029/2008WR007327>, 2010.
- Sebben, M. L., Werner, A. D., Liggett, J. E., Partington, D., and Simmons, C. T.: On the testing of fully integrated surface subsurface hydrological models, *Hydrological Processes*, 27, 1276–1285, <https://doi.org/10.1002/hyp.9630>, publisher: John Wiley & Sons, Ltd, 2013.
- Towler, E., Foks, S. S., Dugger, A. L., Dickinson, J. E., Essaid, H. I., Gochis, D., Viger, R. J., and Zhang, Y.: Benchmarking high-resolution hydrologic model performance of long-term retrospective streamflow simulations in the contiguous United States, *Hydrology and Earth System Sciences*, 27, 1809–1825, <https://doi.org/10.5194/hess-27-1809-2023>, 2023.
- van Verseveld, W. J., Weerts, A. H., Visser, M., Buitink, J., Imhoff, R. O., Boisgontier, H., Bouaziz, L., Eilander, D., Hegnauer, M., ten Velden, C., and Russell, B.: Wflow_sbm v0.7.3, a spatially distributed hydrological model: from global data to local applications, *Geoscientific Model Development*, 17, 3199–3234, <https://doi.org/10.5194/gmd-17-3199-2024>, 2024.
- Vereecken, H., Weihermüller, L., Assouline, S., Šimůnek, J., Verhoef, A., Herbst, M., Archer, N., Mohanty, B., Montzka, C., Vanderborght, J., Balsamo, G., Bechtold, M., Boone, A., Chadburn, S., Cuntz, M., Decharme, B., Ducharne, A., Ek, M., Garrigues, S., Goergen, K., Ingwersen, J., Kollet, S., Lawrence, D. M., Li, Q., Or, D., Swenson, S., de Vrese, P., Walko, R., Wu, Y., and Xue, Y.: Infiltration from the Pedon to Global Grid Scales: An Overview and Outlook for Land Surface Modeling, *Vadose Zone Journal*, 18, 180 191, <https://doi.org/10.2136/vzj2018.10.0191>, 2019.
- Vidal, J.-P., Martin, E., Franchistéguy, L., Baillon, M., and Soubeyroux, J.-M.: A 50-year high-resolution atmospheric reanalysis over France with the Safran system, *International Journal of Climatology*, 30, 1627–1644, <https://doi.org/10.1002/joc.2003>, 2010.
- Virtanen, P., Gommers, R., Oliphant, T. E., Haberland, M., Reddy, T., Cournapeau, D., Burovski, E., Peterson, P., Weckesser, W., Bright, J., van der Walt, S. J., Brett, M., Wilson, J., Millman, K. J., Mayorov, N., Nelson, A. R. J., Jones, E., Kern, R., Larson, E., Carey, C. J., Polat, İ., Feng, Y., Moore, E. W., VanderPlas, J., Laxalde, D., Perktold, J., Cimrman, R., Henriksen, I., Quintero, E. A., Harris, C. R., Archibald, A. M., Ribeiro, A. H., Pedregosa, F., van Mulbregt, P., and SciPy 1.0 Contributors: SciPy 1.0: Fundamental Algorithms for Scientific Computing in Python, *Nature Methods*, 17, 261–272, <https://doi.org/10.1038/s41592-019-0686-2>, 2020.
- Wood, E. F., Roundy, J. K., Troy, T. J., van Beek, L. P. H., Bierkens, M. F. P., Blyth, E., de Roo, A., Döll, P., Ek, M., Famiglietti, J., Gochis, D., van de Giesen, N., Houser, P., Jaffé, P. R., Kollet, S., Lehner, B., Lettenmaier, D. P., Peters-Lidard, C., Sivapalan, M., Sheffield, J., Wade, A., and Whitehead, P.: Hyperresolution global land surface modeling: Meeting a grand challenge for monitoring Earth’s terrestrial water, *Water Resources Research*, 47, <https://doi.org/10.1029/2010WR010090>, 2011.
- Yamazaki, D., Ikeshima, D., Tawatari, R., Yamaguchi, T., O’Loughlin, F., Neal, J. C., Sampson, C. C., Kanae, S., and Bates, P. D.: A high-accuracy map of global terrain elevations, *Geophysical Research Letters*, 44, 5844–5853, <https://doi.org/10.1002/2017GL072874>, 2017.

<https://doi.org/10.5194/egusphere-2025-690>

Preprint. Discussion started: 12 March 2025

© Author(s) 2025. CC BY 4.0 License.



Zhu, C., Byrd, R. H., Lu, P., and Nocedal, J.: Algorithm 778: L-BFGS-B: Fortran Subroutines for Large-Scale Bound-Constrained Optimization., ACM Trans. Math. Softw., 23, 550–560, <http://dblp.uni-trier.de/db/journals/toms/toms23.html#ZhuBLN97>, 1997.